https://doi.org/10.5194/egusphere-2026-3116
Preprint. Discussion started: 3 July 2026

Characterizing observed aerosols and their impacts on shallow cumulus clouds during the TRACER field campaign

Azusa Takeishi[1], Yang Tian[1], Kamal Kant Chandrakar[1], Christina McCluskey[1], Aaron Funk[2], Courtney Schumacher[2], Gregory Roberts[3]

[1]NSF NCAR, Boulder, CO, 80305, U.S.A.
[2]Texas A & M University, College Station, TX, 77843, U.S.A.
[3]Scripps Institute of Oceanography, La Jolla, CA 92093, U.S.A.

Correspondence to: Yang Tian (ytian@ucar.edu)

Abstract. Untangling the role of aerosols in cloud development requires continuous and concurrent measurements of aerosols, clouds, and meteorological conditions. The intensive operational period (IOP) during the U.S. Department of Energy (DOE) Tracking Aerosol Convection Interactions Experiment (TRACER) field campaign provides such datasets. Based on K-means clustering analysis of aerosol data during TRACER-IOP, we found four dominant aerosol clusters present in La Porte, Texas: *Continental* (24%), *Extreme Pollution* (8%), *Sea Breeze and Rural* (45%), and *Sea Breeze and Pollution* (23%). The two *Sea Breeze* clusters are characterized by the inclusion of relatively large particles sized around 180 nm, along with the peak frequency in the afternoon and evening, which are both consistent with the characteristics of sea breeze. These two clusters are a mixture of different aerosol types, which confirms the complexity of aerosol characterization in this region. Utilizing the representative number concentration and size distribution of these aerosol clusters, large eddy simulations of shallow cumulus clouds were performed with the Cloud Model 1. Our comparison of simulated cloud characteristics using a bulk microphysics scheme with those using a Lagrangian scheme (the super-droplet method) reveals that the bulk scheme tends to produce too much precipitation too early, despite the fact that we do not observe surface precipitation from these shallow cumulus clouds of interest, also in contrast to the results with the Lagrangian scheme. This discrepancy is due to the underestimation of droplet number concentrations and/or the overestimation of collision-coalescence rates in the bulk microphysics scheme.

1 Introduction

Over the recent decades, aerosol-cloud interaction (ACI) has been a frequently discussed issue. On the Earth system scale, ACI contributes to the large uncertainty in the radiative forcing with the potential to partially offset the ongoing warming (e.g., Forster et al., 2021; Im et al., 2026). On the weather scale, many observational studies have identified strong controls of aerosols on cloud characteristics for a range of cloud types (e.g., Fan et al., 2016; Li et al., 2025). Among the topics of ACI, the role of aerosols in invigorating convective clouds has been actively examined through observations and modeling (e.g., Rosenfeld et al. 2008; Lebo and Seinfeld, 2011; Fan et al., 2018; Igel and van den Heever, 2021; Öktem et al., 2023; Varble

https://doi.org/10.5194/egusphere-2026-3116
Preprint. Discussion started: 3 July 2026

et al., 2023; Patil et al., 2025), the conclusion of which is usually confounded by the covariability of aerosol, cloud, and meteorological conditions. ACI centers around the fact that aerosols play an important role in cloud formation and development by nucleating cloud droplets (i.e., acting as cloud condensation nuclei, CCN) and/or by initiating ice formation (i.e., acting as ice-nucleating particles, INPs) before homogeneous freezing of liquid occurs at around −38℃. When aerosols' role as CCN and/or INPs is considered, not only the abundance of aerosols but also the size and chemical composition of aerosols are important (e.g., Petters and Kreidenweis, 2007; Pöhlker et al., 2023). To clearly disentangle the contribution of aerosols on cloud development, concurrent measurement of aerosol, cloud, and dynamical characteristics is critical. However, this is challenging and requires a suite of instruments over an extended period of time.

To address such a strong need for extensive and concurrent observations of aerosols, clouds, and dynamical conditions, the Tracking Aerosol Convection Interactions Experiment (TRACER) field campaign (Jensen et al., 2023; Jensen et al., 2025) took place in Southeast Texas around Houston, TX, between October 2021 and September 2022. During the campaign, measurements of aerosols and clouds were made at multiple sites (two ground sites and one mobile facility) over the Greater Houston area, with the overarching aim to deepen our understanding of how background aerosol conditions influence the formation and development of convective clouds. Aerosol conditions in this region are unique and complex: while surrounded by many anthropogenic aerosol emission sources including the megacity of Houston and several oil refineries, the region also experiences sea and bay breezes almost daily during summer months (Wang et al., 2024), which bring in different types of particles into the region.

Based on the mobile facility (Rapid Onsite Atmospheric Measurement Van; ROAM-V) during TRACER, Thompson et al. (2025a) recently summarized the characteristics of aerosols in the region. Their study identified two main aerosol types: polluted maritime and continental aerosols. The former type has a mean concentration of 2500 cm^{-3}, whereas the latter has a mean concentration of 5208 cm^{-3}. Both types are quite "polluted", as a typical clean marine air mass is nominally characterized by much lower concentrations well below 1000 cm^{-3} (e.g., Fitzgerald, 1991; Koponen et al., 2002; Flores et al., 2020). They concluded that the polluted marine air mass includes ship emissions over the Gulf, which raised the aerosol concentrations but not necessarily changed the hygroscopicity of this aerosol mixture. Thompson et al. (2025b) focused on ice nucleation temperature of particles in the Greater Houston area during TRACER to examine the ability of those aerosols to serve as INPs and showed two temperature peaks at T = −24℃ and −15℃, albeit with a large variability in time and space. These studies highlight the complexity of aerosol characteristics in the region, and a further need for aerosol characterization to clarify the ACI in this region.

To understand ACI in the region, recent studies have performed statistical analysis on aerosol and convective cloud properties using the data acquired during TRACER. Al-Jabri et al. (2025) found negative correlation between aerosol abundance and convective cell area but no clear relationship between aerosol and cloud echo-top height. In contrast, Wang et al. (2025) found an increase in echo-top height by about 1 km when ultra-fine particles were present. Huang et al. (2025) found vertical velocity, air temperature, and mass concentration of fine-mode aerosols to be the most important factors to cloud properties using a machine-learning approach. To clarify the physical mechanisms behind these covariances, modeling of ACI

https://doi.org/10.5194/egusphere-2026-3116
Preprint. Discussion started: 3 July 2026

is necessary. Some numerical simulations have been done to disentangle ACI over the Greater Houston area (e.g., Marinescu et al., 2021; Zhang et al. 2021; Subba et al., 2026), but not on the large-eddy simulation (LES) scale that can capture fine variability of cloud structure and microphysical processes, while integrating TRACER-observed aerosol characteristics into simulations.

For modeling clouds, mainly three kinds of microphysics schemes are available in LESs (e.g., Grabowski et al., 2019; Morrison et al., 2020): bulk, bin, and Lagrangian (i.e., particle-tracking). Many studies have been done to compare bulk and bin schemes (e.g., Khain et al., 2015; Sato et al., 2015; Stanford et al., 2025), bin and Lagrangian schemes (e.g., Morrison et al., 2018; Chandrakar et al., 2022; Witte et al., 2022), and bulk and Lagrangian schemes (e.g., Naumann and Seifert, 2015; Sato et al., 2018; Yin et al., 2024). Both bulk and bin schemes suffer from numerical diffusion that potentially leads to erroneous calculations of microphysical processes (Grabowski et al., 2019), which can be mitigated by using a Lagrangian scheme. In addition to the minimalization of artificial numerical diffusion, the major advantages of Lagrangian schemes include the capability to explicitly track the growth process of wet aerosols into cloud droplets, exclusion of assumptions for hydrometeor size distributions, the use of stochastic drop collision-coalescence based on the kernel function, and the elimination of artificial size thresholds for certain cloud processes (Grabowski et al., 2019). On the other hand, simulations with Lagrangian schemes are computationally expensive and may not be affordable in operational forecasts or global models. It is therefore important to assess the difference in cloud properties simulated by a bulk/bin scheme and a Lagrangian scheme, when ACI is discussed.

Over the Greater Houston area, shallow cumulus clouds are the most frequently observed type of cumulus clouds in the summer. Based on a cell tracking algorithm used on radar and satellite data between June and September of 2018-2021, Tuftedal et al. (2024) found that the number of shallow convection cells was more than four and seven times higher than that of the modest and vigorous deep convection, respectively (see their Figure 2 and Table 1). Even though shallow cumulus clouds are common in this region and play an important role in pre-moistening the mid troposphere and setting a stage for deeper cloud developments, the vast majority of studies have so far focused on deeper convective clouds, except for Mages et al. (2025) who performed clustering analysis of satellite and radar data during TRACER and identified four major types of diurnal cycles for shallow cumulus clouds over the region. Additionally, summertime shallow cumulus clouds in the area do not include any ice processes, which simplifies our interpretation of aerosol influence on cloud development. Given the prevalence of shallow cumulus and their role in setting the deep convection stage, more studies on those clouds, especially with respect to their sensitivity to aerosol perturbations, are highly desired.

In response to the above-mentioned points of (1) needs for aerosol characterization over the Greater Houston area, (2) importance of LES-scale modeling in understanding the physical mechanisms behind ACI, (3) significance of comparing simulations with a bulk/bin scheme and a Lagrangian scheme to assess the potential error in ACI estimated by operational forecasting and global models, and (4) the relative lack of studies on the sensitivity of shallow cumulus clouds to aerosols in spite of their high prevalence over the region, this study achieves the following three objectives:

https://doi.org/10.5194/egusphere-2026-3116
Preprint. Discussion started: 3 July 2026

1. Perform unsupervised clustering analysis to characterize and gain insights into the aerosol conditions (abundance, size distribution, timing, origin, etc.) at the main TRACER observation site
2. Run numerical simulations of shallow cumulus clouds on an LES scale while changing available aerosol, based on the aerosol groups found in 1 above, to identify the sensitivity of shallow cumulus clouds to aerosols and clarify the physical mechanisms behind ACI
3. Compare microphysical properties of shallow cumulus clouds simulated by a bulk and a Lagrangian microphysics scheme to assess differences in cloud lifecycle and surface rainfall using bulk schemes

Thus, this study takes a comprehensive approach to achieve these goals, where observational data from TRACER are integrated into LES with the aid of a machine-learning clustering technique.

The rest of the paper is organized as follows: Section 2 describes the methods of the clustering analysis (2.1) and settings of numerical simulations (2.2); Section 3 presents the results of the clustering analysis (3.1), simulations of shallow cumulus clouds with different aerosol clusters with a bulk microphysics scheme (3.2), and the comparison of simulations with bulk and Lagrangian schemes (3.3); and Sect. 4 summarizes the findings and conclusions from the study.

2 Methods

The following two subsections introduce the methodology used for aerosol clustering (Sect. 2.1) and for running numerical simulations of shallow cumulus clouds (Sect. 2.2).

2.1 Aerosol clustering

During the Intensive Operational Period (IOP) of TRACER between June and September 2022, continuous measurements of meteorological conditions and aerosol characteristics were made at the Atmospheric Radiation Measurement (ARM) Mobile Facility 1 (AMF1; longitude: 95.059°W, latitude: 29.67°N) site in La Porte, Texas, at high temporal frequencies (i.e., minutes to hours). A variety of instruments, such as cloud radar, precipitation radar, and a suite of aerosol instruments were deployed at this ground site, as elaborated in greater detail in Jensen et al., (2019).

Given the complex nature of aerosols in this region combined with the large amount of data acquired during the 4-month TRACER-IOP, we characterize aerosols by obtaining statistical descriptions of particles with similar properties through a clustering method. Our clustering generally follows the methodology in Atwood et al. (2019) that was preceded by Atwood et al. (2017), where they used 67 aerosol and meteorological variables obtained from the CalWater-2015 field campaign (Ralph et al., 2016). We utilize the Python scikit-learn function of K-means clustering with random initial centroids and 300 maximum iterations. The clustering result quickly converged after 34 iterations, and therefore varying the maximum iteration number does not have impacts on the clustering result.

As an input of clustering, we use the aerosol data from the ARM Scanning Mobile Particle Spectrometer (SMPS). SMPS provides a number concentration and a size distribution of aerosols in logarithmically spaced 192 bins between 1 nm and 1 μm diameter at approximately 5-minute intervals. The choice of these variables also follows that in Atwood et al. (2019).

https://doi.org/10.5194/egusphere-2026-3116
Preprint. Discussion started: 3 July 2026

We first calculate the normalized size distribution (i.e., number size distribution [$cm^{-3}(dlog_{10}D)^{-1}$] divided by the total concentration [cm^{-3}]) and average the distribution every 4 bins between 10.2 nm and 478.3 nm to result in 27 wider bins. This re-mapping is done to reduce the number of size-distribution variables for clustering to a similar value as that used in Atwood et al. (2019), which was 20. The remapped data is then temporally averaged every 5 minutes for the entire IOP period, which results in 35018 total data points (i.e., 12 × 24h × 122 days) for aerosols when missing data are excluded.

In addition to aerosol data, we utilize meteorological data obtained at the AMF1 site to characterize the air mass origins. Following Atwood et al. (2019), we utilize the wind direction data measured by the surface meteorological instrument (MET) at AMF1 and compute sine and cosine of the data to convert the values ranging from 0 to 360 into two sets of data between -1 and 1. Furthermore, we use the NOAA Air Resources Laboratory (ARL) Hybrid Single-Particle Lagrangian Integrated Trajectory model (HYSPLIT; available at https://www.ready.noaa.gov; Rolph et al., 2017; Stein et al., 2015) to obtain back-trajectories of a surface air mass three and six hours prior to arriving at the AMF1 site. The version of the HYSPLIT data used here is the archive trajectories from the hourly High Resolution Rapid Refresh (HRRR; Dowell et al., 2022) model data with a 3 km horizontal resolution.

The input variables for our clustering analysis are summarized in Table 1. Note that these variables are all standardized (i.e., subtract mean and divide by standard deviation) and weighed differently (see Table 1 for weight values) upon clustering, following Atwood et al. (2019). In their study, the weights of most variables were determined such that the total weight from each data type summed to 1, which is the case in this study as well. In their work and our work, these weight values were experimentally determined through trial and error in efforts to minimize the sum of squared errors (SSE). The final number of data points is 2917 with all 34 variables available; the major data point reduction is due to the lower temporal resolution of the hourly HYSPLIT data.

Table 1: List of input variables for clustering

	Variable	Units	Weight	Data type	Data source
1	Total aerosol number concentration	[cm^{-3}]	1	Aerosol	SMPS
2-28	Normalized number size distribution (size 10.2 - 478.3 nm)	[$(dlog_{10}D)^{-1}$]	$\frac{1}{27}$ each		
29	Cosine (wind direction)	[unitless]	0.5 each	Meteorology	MET
30	Sine (wind direction)				
31	$Longitude_{-3h} - Longitude_{AMF1}$	[degrees]	0.5 each		HYSPLIT
32	$Latitude_{-3h} - Latitude_{AMF1}$				
33	$Longitude_{-6h} - Longitude_{AMF1}$		0.5 each		
34	$Latitude_{-6h} - Latitude_{AMF1}$				

https://doi.org/10.5194/egusphere-2026-3116
Preprint. Discussion started: 3 July 2026

2.2 Numerical simulations of shallow cumulus

Based on the results from the aerosol clustering above, we run LESs of shallow cumulus clouds with different aerosol clusters, using the Cloud Model 1 (CM1; Bryan and Fritsch, 2002). The simulation domain is 12.8 km × 12.8 km (double periodic) with a 50-m horizontal resolution (i.e., 256 points in both x and y directions). The vertical resolution is 30 m with 160 vertical levels from the surface to 4.8 km. For representing subgrid-scale turbulence, the prognostic TKE scheme (Deardorff et al., 1980) is employed. Rayleigh damping is applied to the layer above 4.5 km to avoid the reflection of vertically propagating waves. The simulations use the RRTMG radiation scheme (Iacono et al., 2008). The time step for the calculation of physics is 0.6 s, while that of radiation processes is 10 minutes, and results are output every 5 minutes.We use two microphysics schemes in this study: the Morrison double-moment bulk microphysics scheme (Morrison et al., 2005; Morrison et al., 2009) and the Lagrangian super-droplet method (SDM; Shima et al., 2009). For the comparison of the two schemes, the same observation-derived aerosol size distributions are used to initialize the simulations.

In the Morrison scheme, the background aerosols are fixed over time (i.e., the same number and sizes of aerosols are continuously available in the grid without being scavenged), as no explicit calculations for aerosols are included in the scheme. This means that the entrainment process does not impact the interstitial aerosol availability or size distributions. In this scheme, aerosol activation is based on Abdul-Razzak and Ghan (2000), and autoconversion and accretion are both based on Khairoutdinov and Kogan (2000; see their equations 29 and 33, respectively).

In SDM, microphysical processes of individual “super-droplets” (SDs), each of which carries a weight factor called ‘multiplicity’ (i.e., equivalent to the number of physical particles each SD representsin a given location), are calculated in the Lagrangian framework. Unlike the bulk scheme where unactivated aerosol concentrations are fixed in space and time, the dry aerosol abundance varies with space and time in SDM, which allows for more realistic realization of aerosol evolution in the model. Aerosol particles go through wet growth based on the environmental humidity and get activated into cloud droplets when the environmental supersaturation exceeds aerosols’ critical supersaturation. The collision kernel of Hall (1980) is chosen for this study. The SDM calculation is turned on after 30 minutes of turbulence spinup for the sake of computational efficiency. The timestep for the SDM calculation is 0.15 s, which means that four SDM timesteps are advanced upon one CM1 model timestep. Subgrid-scale velocity fluctuation is accounted for in SDM but subgrid-scale supersaturation fluctuation is not.

We identified a representative shallow cumulus case to simulate during TRACER-IOP, based on our analysis of satellite and variational analysis forcing data. Shallow cumulus clouds on 20 July, 2022, developed in a prevalent southeasterly wind and showed macrophysical features (cloud-base/cloud-top heights and lifecycle) of shallow cumulus clouds in the region. Figure 1a-c shows GOES-16 images (Bah et al., 2018; Schmit et al., 2017; NOAA 2025) on that day, which captures the wide coverage of shallow cumulus clouds in the region, starting at around 8am Local Time (LT; -5 hours UTC) and continuing into the afternoon. A time series of cloud fraction from the hourly ARM Best Estimate (ARMBE, Fig. 1d) for the AMF1 site indicates that the shallow cumulus clouds started developing between 8-9 am LT with a cloud base around 600 m and a cloud

https://doi.org/10.5194/egusphere-2026-3116
Preprint. Discussion started: 3 July 2026

185 depth of a few hundred meters. Cloud base, depth, and fraction increased throughout the morning, reaching a maximum cloud base height of 1.3 km, cloud depth of 1.5 km, and cloud fraction of 35% by 1pm. The cloud height and fraction began decreasing after 2 pm.

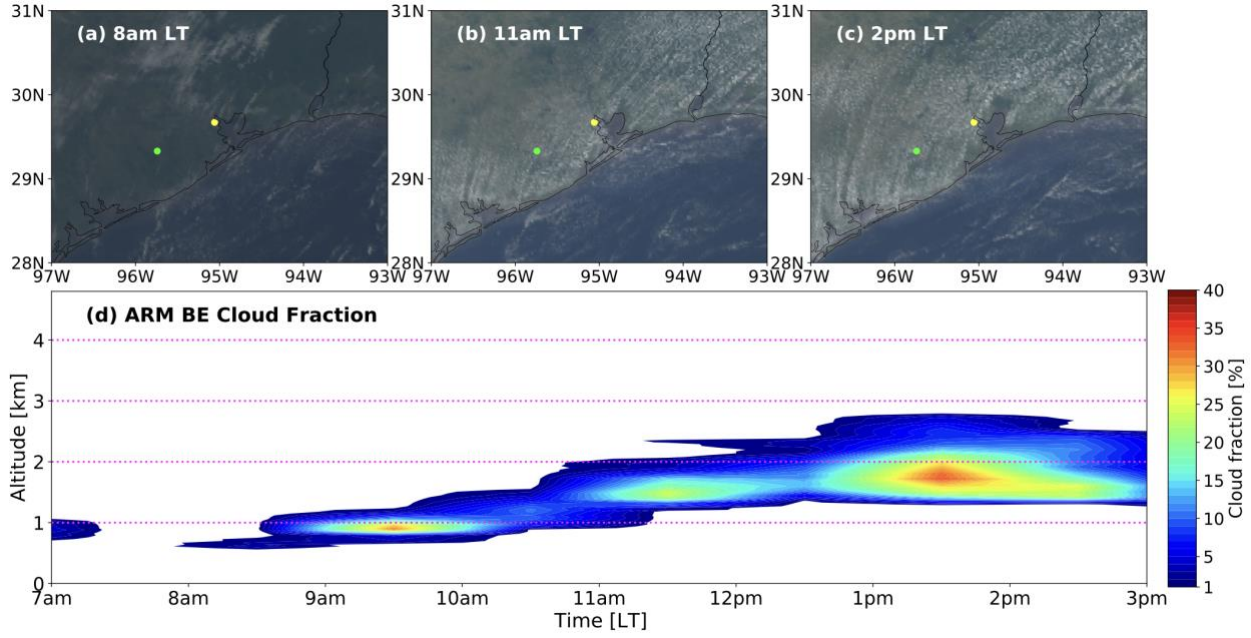

Figure 1: GOES-16 images over the region of interest at (a) 8 am, (b) 11 am, and (c) 1 pm LT on 20 July, 2022. The yellow and green
190 **dots on the maps show the locations of the main site (AMF1) in La Porte and the ancillary site (ANC) in Guy, respectively. (d) Time series of hourly ARMBE cloud fraction [%] observed at AMF1 between 7 am and 3 pm LT on 20 July, 2022.**

To simulate these clouds with CM1, we run the simulations for eight hours, starting at 7am LT. The initial atmospheric profile comes from the variational analysis data at 1200 UTC (i.e., 7am LT). We vary aerosol concentrations with height
195 according to the scaling factor defined in the TRACER Model Intercomparison Project (TRACER-MIP; Saleeby et al., 2025). In SDM, the average number of SDs at the beginning of the simulation is 128 per grid at surface, and this number is also vertically scaled by the same scaling factor from TRACER-MIP. We utilize the hygroscopicity value (Petters and Kreidenweis, 2007) of $\kappa = 0.26$ for all of our simulations; this is the average κ value from the ground-based observations during TRACER-IOP, provided by TRACER-MIP. Generally, κ values vary across different aerosol sources and even within the same airmass,
200 which makes it difficult to identify one representative κ value. Therefore, in this study we focus on the impacts of variability in number and size distributions of aerosols over the area, while the chemical composition represented by κ is set to the mean value of 0.26 across all the simulations. Wind fields are nudged to the variational analysis data every hour. Surface fluxes are also based on the variational analysis data, even though the values are fixed after 8 am LT to keep the boundary-layer height more realistic when compared to observations. We also applied hourly large-scale vertical velocity and heat and moisture

https://doi.org/10.5194/egusphere-2026-3116
Preprint. Discussion started: 3 July 2026

advections to the entire domain throughout the 8-hour simulations. The large-scale advections were modified slightly to better match observations.

3 Results

Results from the aerosol clustering and numerical modeling described in Sect. 2 are presented in this section. The modeling results are split into two. First, comparisons of simulations with the bulk Morrison microphysics scheme under different aerosol conditions (i.e., clusters) are discussed in Sect. 3.2. Next, comparison of two simulation results, one using the bulk scheme and the other with the SDM, both under the same initial aerosol condition, are shown in Sect. 3.3.

3.1 Aerosol clustering

Using the data listed in Table 1, K-means clustering is performed to group the data into K groups. We use the so-called *elbow method* (Thorndike, 1953) and the *Silhouette coefficient* (Rousseeuw, 1987) to find the optimal K value, which best describes the number of clusters that the data can be split into. In the *elbow method*, SSE is first calculated when K is set to a value between 1 and 10. SSE is expected to decrease as K increases, since the number of cluster centers increases and therefore the distance between each point and its cluster center must decrease. When this reduction of SSE with K slows down, the K shows a deflection point where a further increase of cluster number only marginally improves the clustering results. The *Silhouette coefficient* is a measure of how well each data point fits into its assigned cluster, ranging from -1 (closer to another cluster center) to 1 (well in the cluster), the higher the better. Based on these two analyses (see Fig. S1 for further details), we found that the data should be split into either two or four major clusters. Given the strong influence of sea breeze in this region over the summer, K = 2 is expected to split the data into sea-breeze-influenced and uninfluenced clusters, which will miss influencing factors other than sea breeze circulation. We therefore adopt K = 4 for our analysis and present discussions of the results from K-means clustering with K = 4 for the rest of this study.

The data in Table 1 are clustered into four groups, each with distinct characteristics of aerosols and dynamical conditions. Figure 2a shows the frequency of occurrence of each cluster (sum to 100%). Cluster 4 has the highest frequency (45 %), while Cluster 3 has the lowest frequency (8 %). The highest number concentrations are associated with Cluster 3, with a median number concentration exceeding 16,000 cm^{-3} (Fig. 2b). Cluster 1 has the second highest median number concentration of 6544 cm^{-3}, followed by Cluster 2 (3506 cm^{-3}) and Cluster 4 (2231 cm^{-3}). Figure 2c and 2d further describes each cluster's aerosol characteristics. The most "polluted" Cluster 3 includes a lot of small (< 50 nm) particles, which lower the geometric mean diameter (GMD) to 32 nm. The second most "polluted" Cluster 1 has the largest GMD of 45 nm and its median size distribution in Fig. 2d does not show a particular peak at any size. As for Clusters 2 and 4, their GMDs are similar (40 nm and 39 nm, respectively) and they both show a distinct mode of the distribution around 180 nm. Figure 3 shows the wind rose for each cluster. Cluster 1 is dominated by northeasterly winds, Cluster 2 by southwesterly winds, and Cluster 4 by

https://doi.org/10.5194/egusphere-2026-3116
Preprint. Discussion started: 3 July 2026

235 southeasterly winds. Cluster 3 is not associated with any particular wind direction and the wind speed is generally low, which implies the association of this cluster with relatively local air masses.

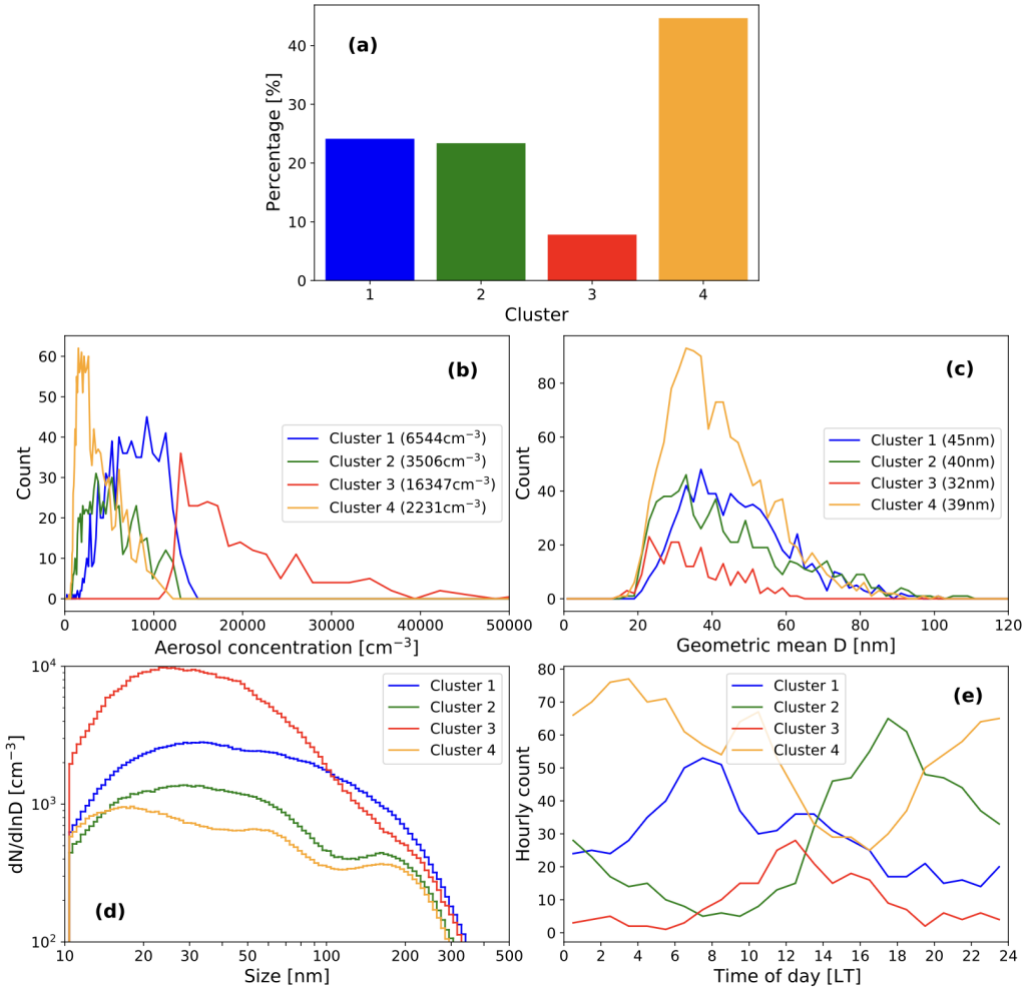

Figure 2: The results of K-means clustering with K = 4 as follows; (a) Percentages [%] of cluster occurrences, (b) counts of SMPS concentrations [cm^{-3}] separated into 100 logarithmic bins between 10^2 and 10^5, (c) counts of SMPS geometric mean diameter [nm]
240 **binned every 2 nm, (d) cluster-median SMPS size distributions [cm^{-3}(dlnD)$^{-1}$], and (e) hourly counts of cluster occurrences. The numbers in the brackets within the legend in (b) and (c) are the cluster-median values.**

https://doi.org/10.5194/egusphere-2026-3116
Preprint. Discussion started: 3 July 2026

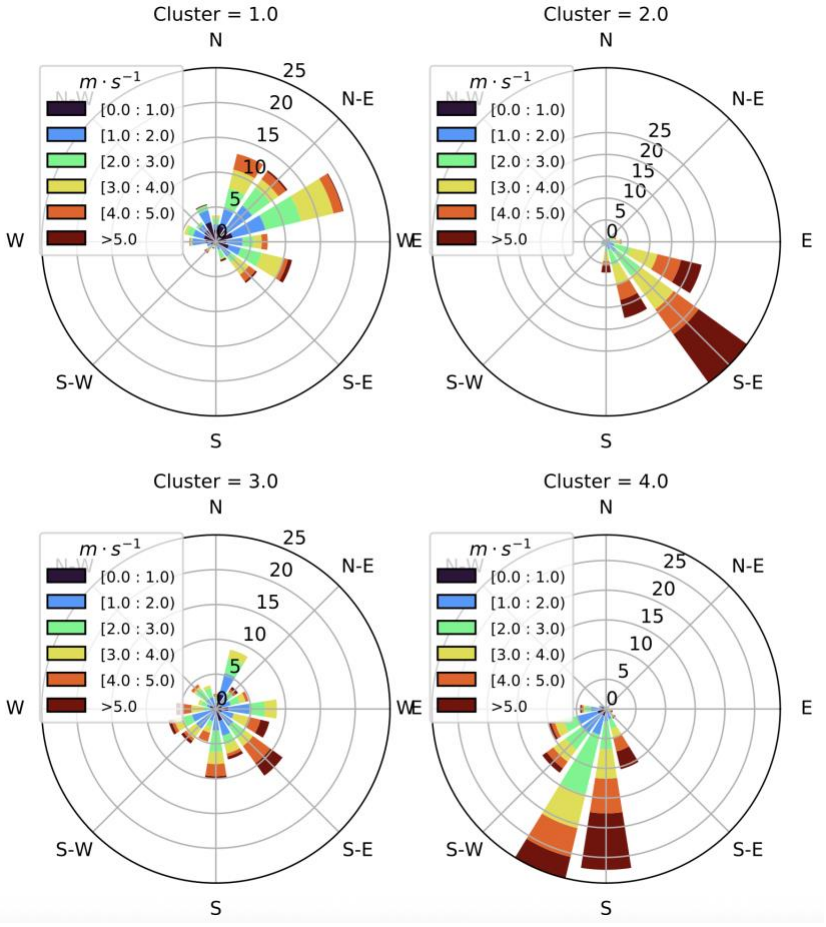

Figure 3: Wind roses of (upper left) Cluster 1, (upper right) Cluster 2, (lower left) Cluster 3, and (lower right) Cluster 4.

Figure 4 shows the locations of air parcels 3 and 6 hours prior to arriving at the AMF1 site based on the HYSPLIT data that was used for the clustering. The majority of air masses in Cluster 1 were over the continent, as expected from the cluster's association with the northeasterly winds (Fig. 3). Therefore, it is appropriate to label this cluster as the continental cluster. As for Cluster 3, there is no particular area where air masses originated from, but Houston and other industrial areas in vicinity with oil refineries and a power plant (Roberts et al., 2026) are included as the locations of origin. Given the extremely high aerosol number concentrations (Fig. 2b) and small aerosol sizes (Fig. 2d) associated with Cluster 3, this cluster includes freshly emitted aerosol particles from anthropogenic and industrial sources nearby, thereby confirming its association with extreme pollution. Compared to Cluster 3, Clusters 2 and 4 both exhibit relatively low aerosol number concentrations (Fig. 2b), similar GMDs (Fig. 2c), and a distinct mode of aerosols sized around 180 nm (Fig. 2d) that are likely associated with sea salt particles from the Gulf. Their distinction mainly lies in the primary wind directions; Figure 4 shows that air masses in Cluster 2 mainly come from the Gulf and the bay, the latter of which is known for high industrial activities. Therefore, it is reasonable to label this cluster as a mixture of sea breeze and pollution particles. Indeed, Cluster 2 has more small (< 50 nm)

https://doi.org/10.5194/egusphere-2026-3116
Preprint. Discussion started: 3 July 2026

particles compared to Cluster 4 (Fig. 2d). On the other hand, air parcels in Cluster 4 originate from the Gulf and the southwest of AMF1, the latter of which is around TRACER's secondary ancillary site (ANC) in Guy, TX, with cleaner "rural" aerosol conditions. Therefore, this aerosol cluster likely includes a mixture of sea breeze and rural particles.

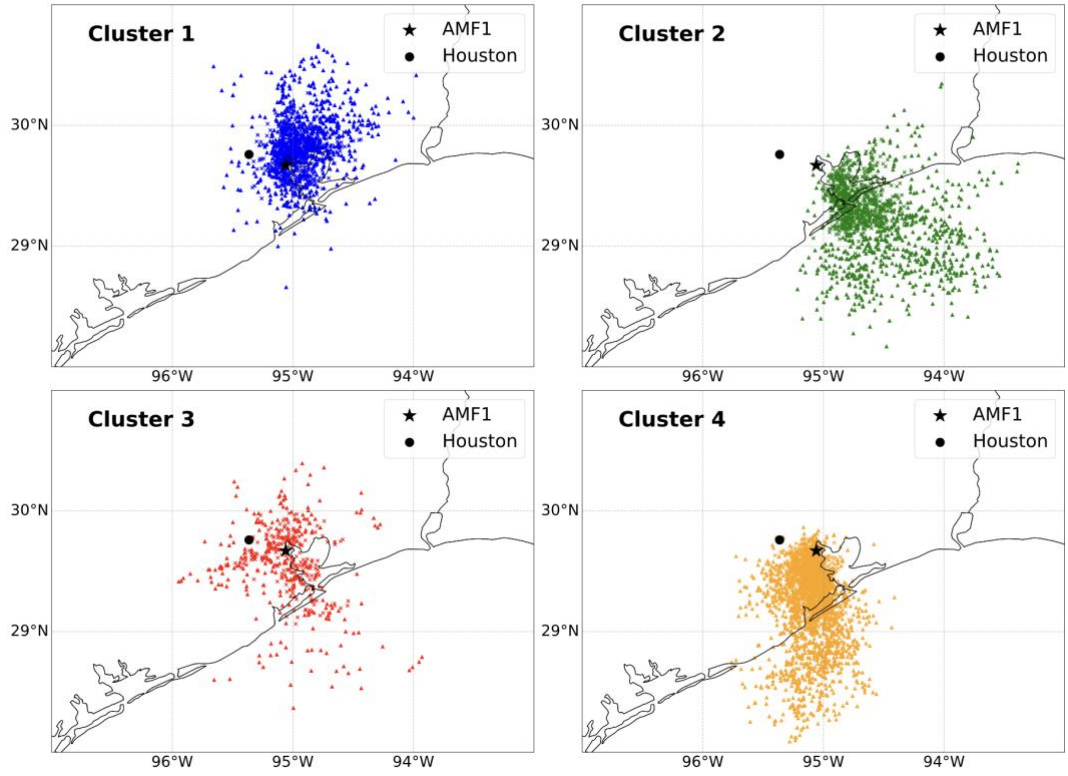

Figure 4: Locations of air masses at 3 hours (×) and 6 hours (▲) prior to their arrivals at the AMF1 site at the ground level (Z = 0 m), based on HYSPLIT, for (upper left, blue) Cluster 1, (upper right, green) Cluster 2, (lower left, red) Cluster 3, and (lower right, orange) Cluster 4.

Based on the combined aerosol and wind characteristics in Figs. 2-4, we name these clusters as follows: Cluster 1 as *Continental*, Cluster 2 as a mixture of *Sea Breeze and Pollution* (or *SB+Pollution*), Cluster 3 as *Extreme Pollution*, and Cluster 4 as a mixture of *Sea Breeze and Rural aerosols* (or *SB+Rural*).

Figure 2e shows the hourly count of four clusters. Although time of day is not an input for the clustering analysis, it is interesting that each cluster has a distinct diurnal pattern. For example, Cluster 3 is most frequently observed midday, whereas the frequency of Cluster 1 peaks in the early morning and Cluster 2 in the early evening. These observations align well with our assigned cluster labels.A continental air mass (i.e., Cluster 1) is more likely to reach the AMF1 site during nighttime/morning when a land breeze strengthens, a local polluted air (i.e., Cluster 3) may be observed at the AMF1 site midday when industrial activities are ongoing and before a sea breeze arrives and brings in a non-local air mass, and a sea-breeze air mass (i.e., Clusters 2 and 4) in the afternoon/evening when a sea breeze prevails. As discussed in Park et al. (2020),

https://doi.org/10.5194/egusphere-2026-3116
Preprint. Discussion started: 3 July 2026

sea breezes propagate faster during nighttime due to less turbulence associated with surface heating, which is consistent with the prevalence of Clusters 2 and 4 in the late afternoon and evening. The smooth size distribution suggests that aerosols in Cluster 1 may be aged and/or from many different sources.

The difference between Clusters 2 and 4 is also noteworthy in Fig. 2e. Cluster 2 is more prevalent in the afternoon, whereas Cluster 4 is more frequently observed in the evening and morning. Higher anthropogenic and industrial activities during daytime is consistent with the dominance of Cluster 2 in the afternoon over Cluster 4. Wind directions in the region also follow the strong diurnal cycle of sea-breeze and land-breeze, albeit their strength varies. It is speculated that Cluster 2 is associated with the gulf breeze and the earlier phase of sea breeze where the wind direction is directly from the Gulf (i.e., southeast) and the timing is in the afternoon, whereas Cluster 4 is related to the later phase of the sea breeze circulation where the flow is slightly weakened (Fig. 3) and the wind direction is affected by complex local interaction between sea breeze, land breeze, and potentially larger-scale flows.

Using these four identified aerosol clusters from the AMF1 site, we run LESs with the CM1model to assess the impacts of different aerosol conditions on cloud microphysical processes and cloud characteristics.

3.2 Numerical simulations of shallow cumulus: Role of aerosols in bulk microphysics scheme

The numerical simulations with the Morrison bulk microphysics scheme are performed and compared to assess the sensitivity of the shallow cumulus clouds to changes in background aerosols. Microphysical properties of the clouds such as cloud mass, cloud droplet number concentrations (CDNCs), and process rates are examined. The aerosol size distributions shown in Fig. 2d are used for our CM1 simulations of shallow cumulus clouds observed on 20 July, 2022. The dominant aerosol cluster for this day was Cluster 4 (i.e., *SB+Rural*), and the observed size distribution (black) resembles the median distribution of Cluster 4 (orange) in Fig. 5. We perform three CM1 simulations with the median size distributions for Clusters 1-3, and one with the observed (i.e., “Total Observed”) size distribution (black in Fig. 5) that represents Cluster 4. The detailed properties of these 3-mode lognormal size distributions adopted in our simulations, along with the CM1 simulations performed with certain aerosol clusters, are listed in Table 2.

https://doi.org/10.5194/egusphere-2026-3116
Preprint. Discussion started: 3 July 2026

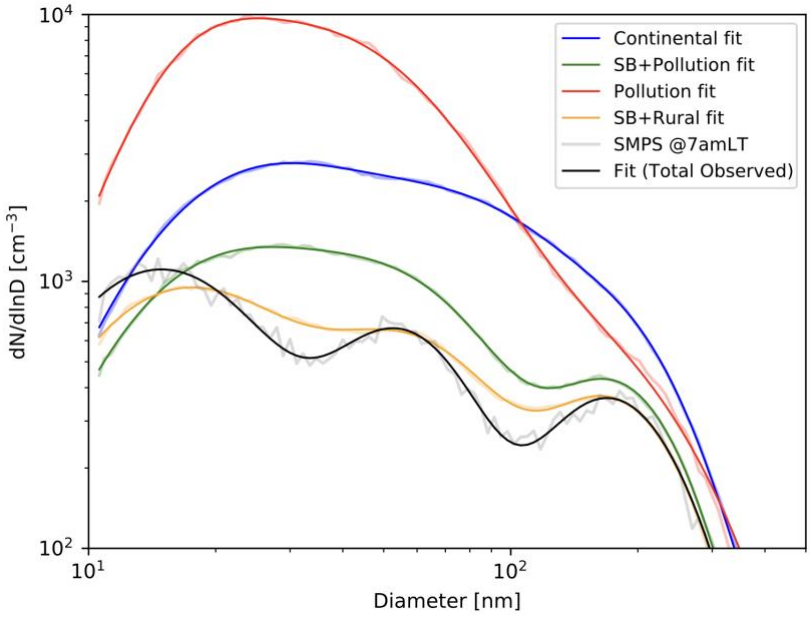

Figure 5: Aerosol size distributions for Clusters 1-4 (blue, green, red, and orange) where three-mode lognormal size distributions are fitted to the cluster-median size distributions shown in Fig. 2d (plotted in faint lines in this figure). The grey and black lines show the SMPS-observed size distribution at 7am LT on 20 July, 2022, and its 3-mode lognormal fit, respectively.

Table 2: Parameters for the three-mode lognormal size distributions shown in Fig. 5. The rightmost column shows the CM1 simulations performed in this study using the bulk and/or SDM microphysics scheme. All numbers are rounded to two significant digits.

Cluster	Name	Concentration [cm^{-3}]			GMD [nm]	Geometric standard deviation	CM1 simulation
		Total	SMPS range (observed)	Mode 1-3	Mode 1-3	Mode 1-3	
1	Continental	6084.23	5917.18 (5917.06)	3129.59	24.77	1.71	Bulk scheme
				2798.35	74.16	1.81	
				156.29	189.59	1.33	
2	Sea breeze + Pollution	2852.80	2728.10 (2729.05)	1511.44	21.38	1.68	Bulk scheme
				1027.34	53.89	1.60	
				314.02	176.73	1.38	
3	Extreme Pollution	15946.76	15476.73 (15473.17)	2103.41	18.75	1.36	Bulk scheme
				13381.50	32.65	1.85	
				461.85	160.49	1.57	
4	Sea breeze + Rural	2151.71	1939.71 (1939.30)	1238.05	17.15	1.69	-
				619.18	57.39	1.54	
				294.47	172.81	1.40	
(Included in Cluster 4)	Total Observed	2226.59	1908.74 (1910.73)	1360.55	14.84	1.63	Bulk scheme SDM
				554.18	54.60	1.42	
				311.86	170.72	1.41	

https://doi.org/10.5194/egusphere-2026-3116
Preprint. Discussion started: 3 July 2026

Simulated domain averaged cloud cover (Fig. 6a-d) for each simulation is generally comparable to the observations of cloud fraction at AMF1 (Fig. 1d). This consistency validates our shallow cumulus case selection for a representative cloud condition over the entire domain. Comparing Fig. 1d and Fig. 6a-d, the major macrophysical characteristics of observed shallow cumulus clouds are captured in the bulk simulations: (1) The initial cloud development started at around 8am LT, (2) cloud-base height increases with time from ~500 m to 1.5-2 km, (3) cloud depth increases with time, and (4) the maximum cloud depth is reached in the early afternoon. Although the maximum cloud top height is overestimated by 500 m in the simulations (i.e., ~3.5 km in comparison to ~3 km as observed), the characteristics of the simulated shallow cumulus clouds generally correspond well with the observed cloud system.

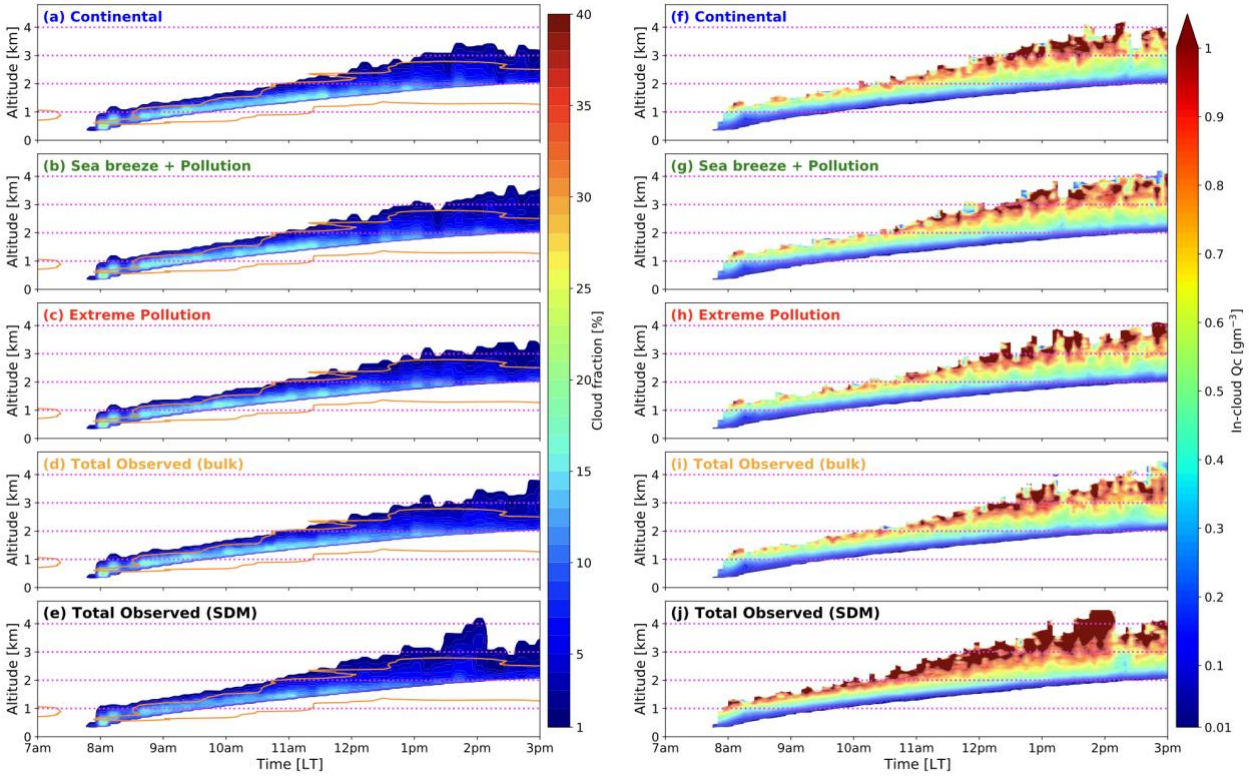

Figure 6: (a-e) Domain-mean cloud fraction [%] and (f-j) in-cloud-mean cloud liquid mass [gm^{-3}] in the CM1 simulations using the Morrison bulk microphysics scheme with (a,f) Continental, (b,g) Sea breeze + Pollution, (c,h) Extreme Pollution, (d,i) Total Observed aerosols, and using (e,j) the SDM. Here "in-cloud" is defined as grids with cloud liquid mass [gm^{-3}] greater than or equal to 0.01 gm^{-3}. The orange line in (a)-(e) shows the cloud fraction contour from the observation in Fig. 1d.

Following cloud fraction in Fig. 6a-d, we first examine the bulk properties of the simulated clouds. In the bulk microphysics simulations (Table 2), in-cloud-mean cloud mass [gm^{-3}] does not vary much among simulations (Fig. 6f-i; see Fig. S2 for domain mean). This is an expected outcome from simulations with bulk microphysics schemes that use saturation

https://doi.org/10.5194/egusphere-2026-3116
Preprint. Discussion started: 3 July 2026

adjustment, where any water vapor above the saturation level is immediately converted into liquid. On the other hand, variation of in-cloud-mean CDNC [cm^{-3}] across simulations is evident (Fig. 7a-d; see Fig. S3 for domain mean). The CDNC variation can be simply explained by the variation in aerosol number concentration; the more available aerosol particles, the higher the domain-mean CDNC (i.e., CDNC increases in the order of SB+Rural and/or Total Observed, SB+Pollution, Continental, and Extreme Pollution). Another bulk property that characterizes the simulated clouds is rain mass. Domain mean rain mass, shown in Fig. 7f-i, varies substantially across the simulations using the bulk microphysics scheme. Comparing the left and right columns of Fig. 7, one pattern is evident among the four simulations: the higher the mean CDNC, the lower the rain mass. This pattern of suppressed rain formation with increased aerosols is expected as a part of the so-called lifetime effect of aerosols (Albrecht et al., 1989). Indeed, autoconversion rates are inversely proportional to CDNC (i.e., $\propto CDNC^{-1.79}$) in the autoconversion parameterization in Khairoutdinov and Kogan (2000) used in this study. Note here that, while the individual cell lifetime may be affected by the loss of water through precipitation, the "system-wide" lifetime of the simulated shallow cumulus clouds, represented in Fig. 6f-i, seems unaffected. This can be explained by the predominant control of the meteorological conditions, including surface fluxes, on the formation and maintenance of these shallow cumulus clouds.

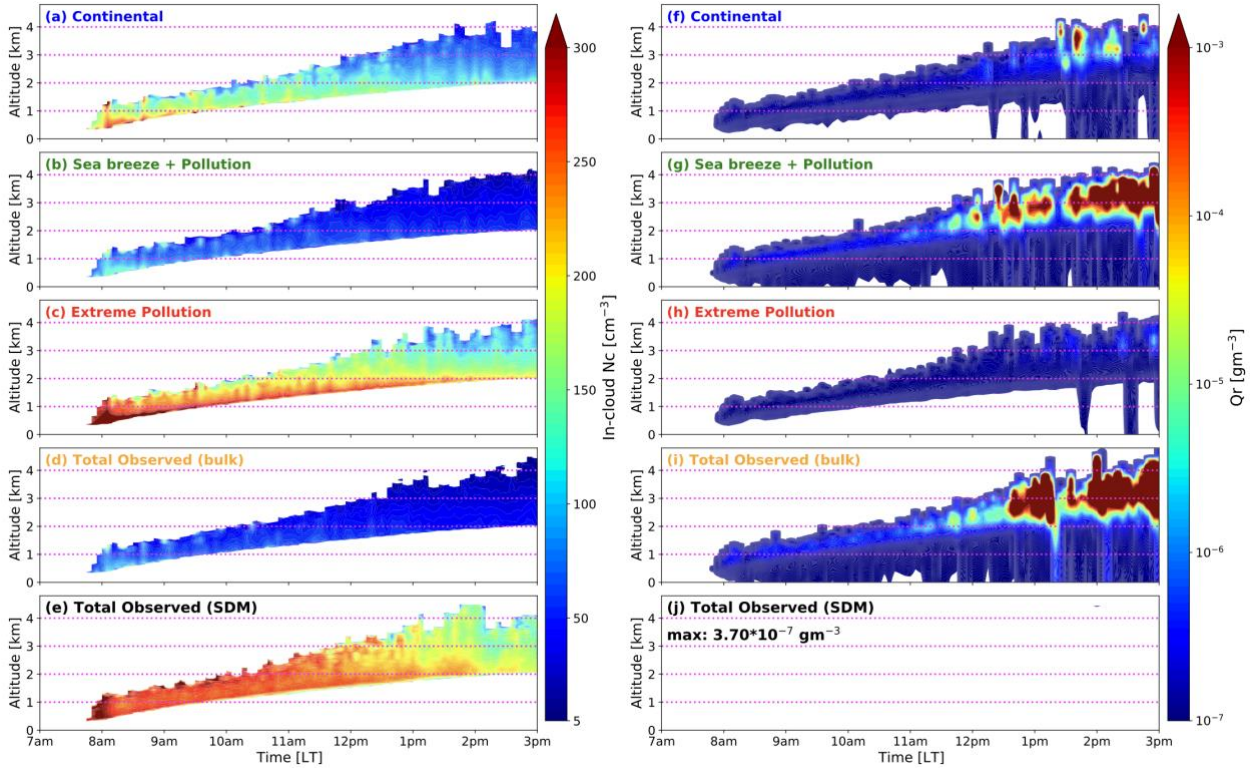

Figure 7: Same as Fig. 6 but for (a-e) in-cloud-mean CDNC [cm^{-3}] and (f-j) domain-mean rain mass [gm^{-3}].

We now examine cloud process rates that explain the differences in cloud bulk properties among the simulations. In-cloud-mean droplet nucleation rates [$cm^{-3}s^{-1}$] in Fig. 8a-d do not linearly correspond to the overall CDNC patterns in Fig. 7a-

https://doi.org/10.5194/egusphere-2026-3116
Preprint. Discussion started: 3 July 2026

d, which confirms that it is not only droplet nucleation but also droplet sink terms (i.e., evaporation and conversion into raindrops) that determine CDNCs. Droplet nucleation rates are the highest in the Continental case (Fig. 8a), because it has the highest number of large (> 100 nm) particles (Fig. 5). Nevertheless, droplet concentrations are the highest in the Extreme Pollution case (Fig. 7c), suggesting the large loss of droplet *number* in the Continental case, most likely through droplet-to-raindrop conversion as evaporation rates are similar in all simulations (Fig. S4). This is supported by Fig. 8f-i that shows indeed the droplet-to-raindrop conversion rates in *mass* [$gm^{-3}s^{-1}$] are higher for the Continental case (Fig. 8f) compared to the Extreme Pollution case (Fig. 8h). This explains why the overall CDNC is higher in the Extreme Pollution case (Fig. 7c) despite the lower nucleation rates (Fig. 8ch). Earlier raindrop formation is evident in the two "cleaner" cases with sea breeze aerosols (Fig. 8g,i). These results are consistent with the patterns of rain mass shown earlier in Fig. 7g,i.

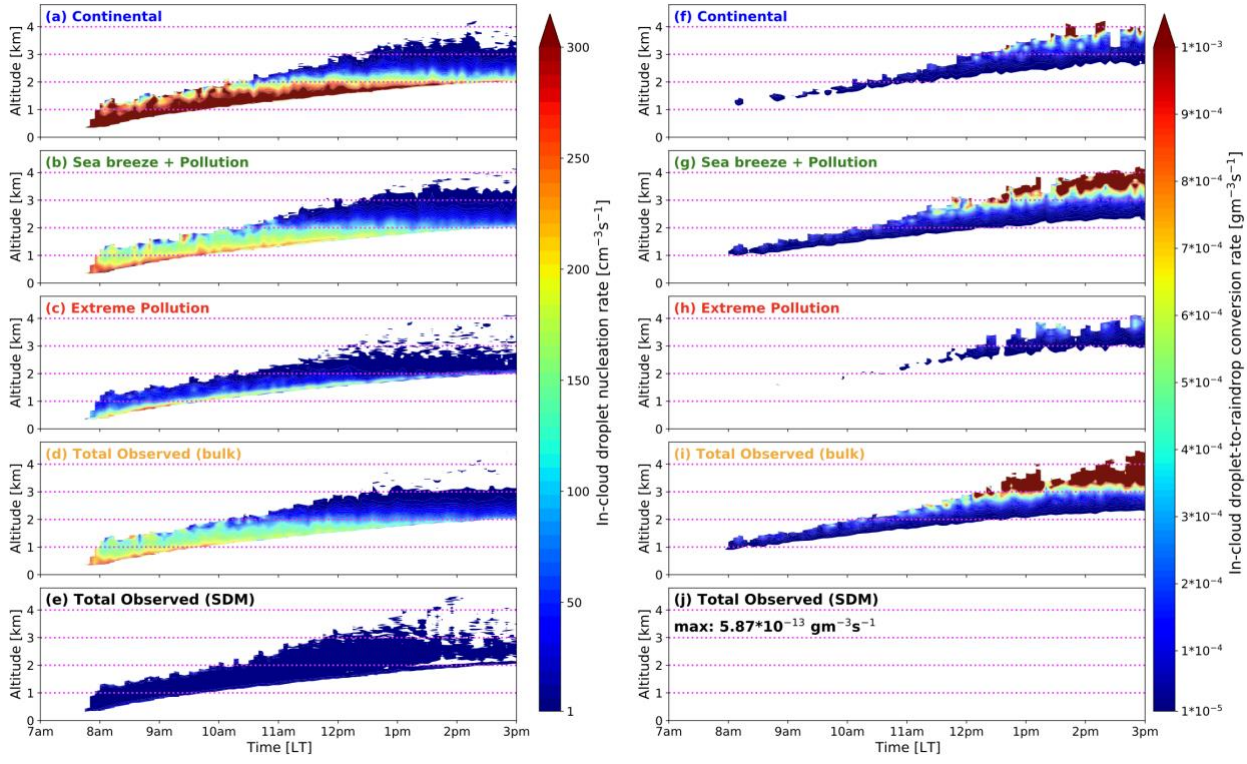

Figure 8: Same as Fig. 6 but for in-cloud-mean (a-e) droplet nucleation rate [$cm^{-3}s^{-1}$] and (f-j) droplet-to-raindrop conversion rate [$gm^{-3}s^{-1}$].

When the time series of domain-mean surface rainfall rates are examined in Fig. 9, the patterns that we see in Fig. 7f-i are confirmed, and even the accumulated amount of surface rainfall corresponds inversely with the number of aerosols in the simulations; the fewer aerosols, the more surface rainfall. This further confirms the presence of the aerosol lifetime effect on the shallow cumulus clouds in our CM1 simulations with the bulk microphysics scheme.

https://doi.org/10.5194/egusphere-2026-3116
Preprint. Discussion started: 3 July 2026

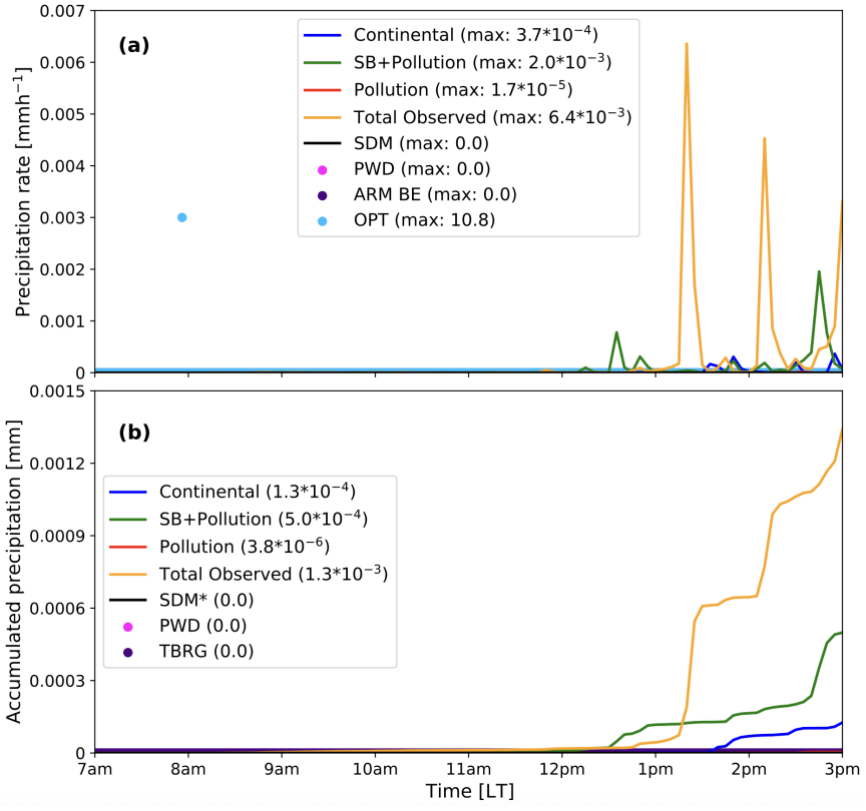

Figure 9: Time series of (a) surface precipitation rate [mmh^{-1}] and (b) accumulated surface precipitation [mm]. The simulation results are domain-mean values. The numbers in the brackets within the legends are the rounded maximum and final values in (a) and (b), respectively. Observed values are shown in markers; PWD stands for Vaisala Present Weather Detectors data in the MET data (every minute), ARMBE (hourly), and OPT for Optical Rain Gauge data and TBRG for Tipping Bucket Rain Gauge data both in the MET data (every minute). Note that the two highest precipitation rates of 10.8 mmh^{-1} and 0.076 mmh^{-1} recorded by OPT at 1:55pm LT and 7:57am LT, respectively, are out of the y-axis scale here. *The SDM values in (b) are indicated values from (a), as accumulated precipitation is not directly available as an output.

3.3 Numerical simulations of shallow cumulus: Role of aerosols in bulk vs. Lagrangian microphysics schemes

We now focus on assessing the difference in cloud properties simulated with the bulk microphysics scheme and SDM, both with the same aerosol properties of the Total Observed aerosol size distribution and number concentration. Given the major advantages of using SDM over bulk schemes as outlined in Sect. 1, we aim to assess the shallow cumulus cloud features and processes in the bulk simulation where the scheme includes limited details but is more widely used for research and forecasting.

The bottom panels of Figs. 6-8 show the results from the SDM simulation with the Total Observed aerosol size distribution (i.e., black in Fig. 5). Cloud fraction in the SDM run, shown in Fig. 6e, is similar to that in the bulk runs (Fig. 6a-d), which signifies the primary control of dynamical conditions on the cloud macrophysical features for the simulated shallow

https://doi.org/10.5194/egusphere-2026-3116
Preprint. Discussion started: 3 July 2026

cumulus clouds, as opposed to the strong influence from microphysics. While the macrophysical features of the clouds are relatively unimpacted by the choice of microphysics schemes, their microphysical characteristics are strongly impacted as evident in Fig. 6i-j. In-cloud-mean cloud mass is 29% higher on average in the SDM run throughout the simulation, which suggests "thicker" clouds therein and is somewhat counterintuitive given the use of saturation adjustments in the bulk scheme that convert all supersaturated water vapor into liquid. This tendency of lower cloud mass in the bulk run, alternatively, can be a result of numerical diffusion. A similar result of lower cloud mass in the Eulerian bin microphysics scheme, compared to SDM, was reported in Chandrakar et al. (2022) and attributed to numerical diffusion in the Eulerian scheme.

As in Sect. 3.2, we first focus our comparison on the bulk cloud properties. In-cloud CDNCs are very different between the bulk run (Fig. 7d) and the SDM simulation (Fig. 7e). The SDM run has more than five times higher in-cloud CDNCs on average throughout the eight-hour simulation. This difference is another counterintuitive discrepancy between the two simulations given that the bulk simulation gets an infinite supply of aerosols while the availability of aerosols is limited in the SDM run (i.e., Sect. 2.2). An even larger difference between the bulk and SDM simulations is evident in rain mass, as shown in Fig. 7i-j. In the SDM run, non-zero rain mass is present in the atmosphere, yet its amount is orders of magnitude less than that in the bulk and the rain does not reach the ground (Fig. 9). In contrast, all the bulk runs seem to have surface rainfall, while the amount varies. These bulk properties of the clouds in the SDM run still technically follow the pattern of "more aerosols, less rain" found in the bulk simulations (Sect. 3.1), but the rain mass difference between the bulk and SDM is substantially larger than those among the bulk simulations. Observed values of surface rainfall rates [mm h^{-1}] and accumulated precipitation [mm] are also shown in Fig. 9. These values come from the hourly ARMBE and the Vaisala Present Weather Detectors (PWD), the Optical Rain Gauge (OPT), and the Tipping Bucket Rain Gauge (TBRG) data in the MET data (every minute). The observed precipitation rates and accumulated precipitation rates are mostly zero, which further confirms the reliability of the SDM simulation results. However, a single pulse of surface rainfall was recorded by the OPT (light blue in Fig. 9a) at around 8 am and 1:55 pm LT, which are considered outliers.

Now we compare cloud process rates to explain the differences in the cloud properties above. Interestingly, Fig. 8e shows a few orders of magnitude lower in-cloud droplet nucleation rates in the SDM run in comparison to the bulk run (Fig. 8d). This tendency is seen throughout the simulation period, which is probably due to the continuous supply of aerosols in the bulk run. It also signifies that the activated droplets continuously get "lost" in the bulk runs after getting activated, either by evaporation or conversion into raindrops, and this is why the activation rate in the bulk simulation remains much higher than that in the SDM run for eight hours, rather than showing the difference only at the initial cloud formation. Consistent with this expectation, in-cloud-mean droplet-to-raindrop *mass* conversion rates in the SDM run shown in Fig. 8j are much lower than that in any of the bulk runs (Fig. 8f-i) throughout the simulations. Though bulk scheme does not output droplet number loss directly, additional analysis suggests that droplet loss through both evaporation and autoconversion play a role here.

Figure 10 compares aerosol concentrations in the bulk simulation using the Total Observed aerosol input (orange; unchanged throughout the simulation) and those in the CM1-SDM run (black box-and-whisker plots). The figure clearly presents the lower aerosol concentrations in CM1-SDM near the cloud base (< ~1.5 km) compared to the bulk run. Interestingly, however,

https://doi.org/10.5194/egusphere-2026-3116
Preprint. Discussion started: 3 July 2026

aerosol concentrations are higher in CM1-SDM above ~2 km, especially later in the simulation. This tendency is more pronounced in the updraft (blue in Fig. 10) where cloud developments are likely. It is likely that these are unactivated aerosol particles lifted from below cloud base and may play a role if these clouds were to develop further into cumulus congestus and deep convection. This topic of aerosol recirculation within the vertically developing cumulus clouds will be addressed in our forthcoming work.

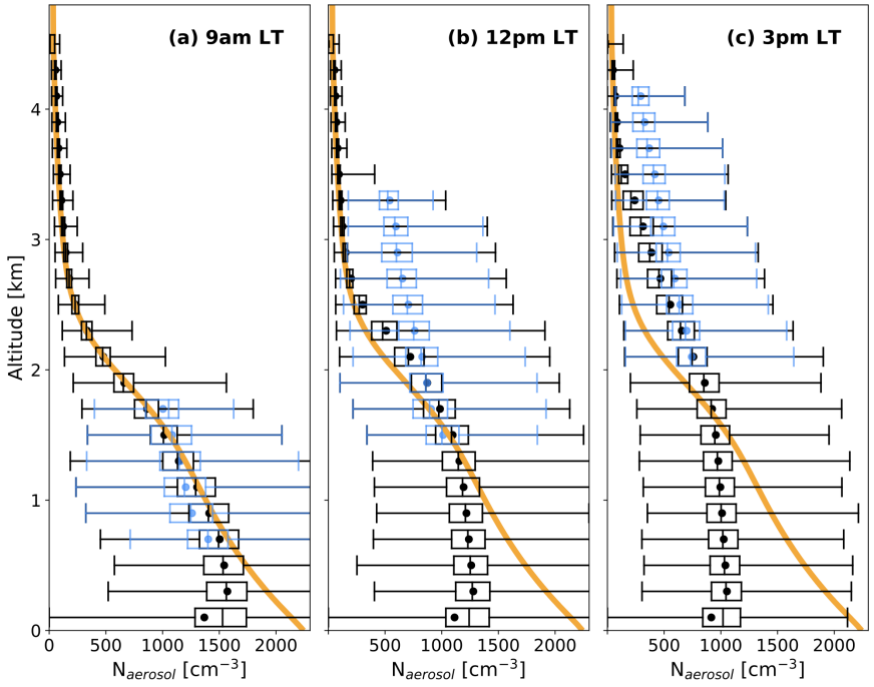

Figure 10: Vertical profile of aerosol concentration [cm^{-3}] in the CM1 bulk-microphysics simulation with the Total Observed aerosols (orange; unchanged throughout the simulation), along with the box-and-whisker plots of in-cloud (Qc > 0.0) aerosol concentrations from the CM1-SDM simulation (black; all domain) binned every 200 m in altitude at (a) 9am, (b) 12pm, and (c) 3pm LT. The blue box-and-whisker plots show the statistics from grid points with updrafts (> 0.1 ms^{-1}) and non-zero cloud mass (i.e., Qc > 0.0) to represent aerosols in areas with a potential cloud development.

Considering SDM represents microphysical processes in significant detail, and likely more realistically than the bulk scheme, it is fair to conclude that the surface rainfalls seen in some of the bulk simulations are overestimations, caused by the overestimated autoconversion/collision-coalescence (droplet-and-droplet collision) and/or accretion (droplet-and-raindrop collision) rates in the bulk scheme. From our results, it is unclear whether the overestimation of droplet-to-raindrop conversion in the bulk scheme occurs due to (1) a deficiency in the representation of droplet activation rates and CDNC (Fig. 7a-d), which leads to higher collision-coalescence rates, (2) structural limitation and parametric uncertainties in the parameterizations of autoconversion and accretion, or (3) both (1) and (2). Since observations provide bulk cloud properties but not process rates, we cannot obtain confirmation of (1), (2), or (3) from observations. Nevertheless, our comparison of the results from the bulk

https://doi.org/10.5194/egusphere-2026-3116
Preprint. Discussion started: 3 July 2026

runs and the SDM run provides an example of a bulk microphysics scheme, often used in larger-scale models and for operational forecasting, erroneously producing rainfalls from shallow cumulus clouds, especially in relatively polluted conditions (e.g., Thompson et al., 2025a).

Overestimation of surface rainfall in an Eulerian scheme in comparison to a simulation with the SDM, along with the earlier onset of precipitation, was previously reported by Chandrakar et al. (2022), although their work assessed a bin scheme rather than a bulk. They attributed the overestimation of rain in the bin scheme to a wider droplet size distribution therein, caused by numerical diffusion. Morrison et al. (2018) also reported such size-distribution broadening by numerical diffusion in a bin scheme. It is therefore critical to assess the validity of bulk simulation results and identify the reason for their discrepancy from the observation-constrained (Sect. 2.2) Lagrangian simulations. Based on our study, along with a recent study by Allwayin et al. (2024) who presented observational evidence of locally much narrower droplet size distributions than a wider gamma-like size distribution when averaged over time, we conclude our simulation results are likely due to any/all of (1)-(3) stated above. To resolve this issue, we need (a) an assessment of the validity of structural choices in bulk microphysics schemes, including a droplet activation parameterization and a gamma size distribution for droplets, through comparisons with in-situ data as in Allwayin et al. (2024), and (b) a rigorous evaluation of assumptions embedded in autoconversion/collision-coalescence and/or accretion parameterizations in bulk microphysics schemes through comparisons with high-resolution in-situ observations under different cloud conditions, controlled laboratory experiments such as cloud-chamber experiments, and/or with observationally constrained detailed microphysics schemes/models, such as high-resolution LES with a Lagrangian microphysics scheme, in the future.

4 Conclusions

This study utilizes the four-month-long observational data from the TRACER field campaign IOP to classify air masses arriving at the AMF1 observation site near Houston, TX, into groups with similar wind and aerosol characteristics. Using a K-means clustering approach, we identify four dominant aerosol clusters. The four clusters are named after their characteristics as follows; (1) *Continental*: mostly coming from the land region to the northeast of AMF1 commonly in the early morning, the aerosols in this cluster show moderately high concentrations with generally large sizes, (2) *Sea breeze + Pollution*: brough to the AMF1 site by strong southeasterly winds from the Gulf, this cluster includes both large marine particles and freshly emitted small aerosols from the industrial bay area in the late afternoon, (3) *Extreme Pollution*: with the most notable characteristics of having extremely high aerosol concentrations and generally small aerosol sizes, particles in this cluster come from the polluted regions in the vicinity in all directions during the daytime when the industrial activity heightens, and (4) *Sea breeze + Rural*: this most commonly observed cluster is characterized by strong southerly/south-southwesterly winds that bring large marine particles from the Gulf and smaller aerosols in the rural area to the southwest of AMF1 (i.e., around TRACER's ancillary site ANC in Guy, TX) in the evening/morning.

https://doi.org/10.5194/egusphere-2026-3116
Preprint. Discussion started: 3 July 2026

Using the distinct aerosol concentrations and aerosol size distributions for these clusters, four CM1 simulations with a bulk microphysics scheme are run and compared to each other for a shallow cumulus clouds case. Our comparison shows a strong impact of aerosol abundance on the raindrop formation processes, where higher aerosol concentrations reduce autoconversion and accretion rates and hence raindrop/rainfall formation as well, as expected from the classic aerosol lifetime effect. On the other hand, comparison with the run with the Lagrangian microphysics scheme (SDM) and the lack of observed rainfall indicates that the simulated droplets-to-raindrop conversion rates in the bulk runs are too high, and therefore, the surface rainfall from these simulated shallow cumulus clouds are likely unrealistic. The most probable reasons for the overestimated raindrop formation rates in the bulk runs are (1) underestimated CDNCs, which leads to higher autoconversion/collision-coalescence rates, and (2) erroneous calculations/parameterizations of autoconversion/collision-coalescence and/or accretion process.

This study demonstrates the applicability of the K-means clustering method to *continuous* observations of aerosols and clouds in characterizing air masses arriving at a particular point. Even under the complex environment where multiple aerosol sources coexist in the vicinity, such as the AMF1 site near Houston, the patterns of air masses are successfully identified through clustering, where two out of the four clusters are likely a mixture of multiple aerosol types (i.e., Sea breeze + Pollution, Sea breeze + Rural). Another highlight of this work is the strong impact of aerosol characteristics and choice of microphysics scheme on precipitation formation in shallow cumulus clouds. A re-evaluation of some assumptions related to aerosols and clouds in microphysics schemes is needed to faithfully represent cloud and precipitation in models. Furthermore, using a horizontally variable aerosol composition to represent spatially inhomogeneous aerosol sources in future work may reveal more complex aerosol-cloud interactions in the region.

Code and data availability

All the TRACER observational datasets analyzed in this study are publicly available at https://www.arm.gov/research/campaigns/amf2021tracer. The GOES-16 images can be made with the data available at https://registry.opendata.aws/noaa-goes, using the example code available at https://unidata.github.io/python-gallery/examples/mapping_GOES16_TrueColor.html. The HYSPLIT data can be obtained at https://www.ready.noaa.gov. The CM1 model is also publicly available for download at https://github.com/NCAR/CM1. The vertical distribution of aerosols for TRACER-MIP, used in this study, is described in detailed at https://arm-synergy.github.io/tracer-mip/Roadmap.html. The simulation data are available at https://www.doi.org/10.5281/zenodo.20348438.

Supplement link

Supplementary figures are available in a separate file.

https://doi.org/10.5194/egusphere-2026-3116
Preprint. Discussion started: 3 July 2026

Author contributions

YT conceptualized the project, acquired funding, and supervised the overall progress of the project. AT carried out the analysis, performed the numerical simulations, visualized the results, and prepared the original draft of the manuscript. KC supervised the design, code, and execution of the numerical simulations. YT, KC, CM, AF, CS, and GR contributed to the discussions of the results and the revision of the manuscript.

Competing interests

The authors declare that they have no conflict of interest.

Disclaimer

Copernicus Publications remains neutral with regard to jurisdictional claims made in the text, published maps, institutional affiliations, or any other geographical representation in this paper. While Copernicus Publications makes every effort to include appropriate place names, the final responsibility lies with the authors. Views expressed in the text are those of the authors and do not necessarily reflect the views of the publisher.

Acknowledgements

This material is based upon work supported by the National Science Foundation (NSF) National Center for Atmospheric Research (NCAR), which is a major facility sponsored by the U.S. National Science Foundation under Cooperative Agreement No. 1852977. This work was funded by the Department of Energy (DOE) grant number DE-SC0024081. G. Roberts acknowledges funding from the NSF grant number AGS-2019965. The authors acknowledge the NOAA Air Resources Laboratory (ARL) for the provision of the HYSPLIT transport and dispersion model and/or READY website (https://www.ready.noaa.gov) used in this publication. We also would like to thank the TRACER observation teams for making the valuable data publicly available and the TRACER-MIP leading team (Jiwen Fan and Steven Saleeby) for compiling the findings to facilitate the modeling work for TRACER. Moreover, we would like to acknowledge high-performance computing support from the Derecho system (doi:10.5065/qx9a-pg09) provided by the NSF NCAR, sponsored by the National Science Foundation. Finally, this research used resources of the National Energy Research Scientific Computing Center (NERSC), a Department of Energy User Facility using NERSC award BER-ERCAP 0037370.

https://doi.org/10.5194/egusphere-2026-3116
Preprint. Discussion started: 3 July 2026

References

Abdul-Razzak, H., and Ghan, S. J.: A parameterization of aerosol activation: 2. Multiple aerosol types, J. Geophys. Res., 105(D5), 6837–6844, https://doi.org/10.1029/1999JD901161, 2000.

Albrecht, B.A.: Aerosols, Cloud Microphysics, and Fractional Cloudiness, Science, 245, 1227-1230, https://doi.org/10.1126/science.245.4923.1227, 1989.

Al-Jabri, A., Lebo, Z. J., and Wang, D.: Investigating Aerosol and Meteorological Influences on Convective Clouds in Houston, Texas, during the TRACER/ESCAPE Field Campaigns, J. Atmos. Sci., 82, 2469–2489, https://doi.org/10.1175/JAS-D-25-0004.1, 2025.

Allwayin, N., Larsen, M.L., Glienke, S., and Shaw, R.A.: Locally narrow droplet size distributions are ubiquitous in stratocumulus clouds, Science, 384, 528-532, https://doi.org/10.1126/science.adi5550, 2024.

Atwood, S. A., Reid, J. S., Kreidenweis, S. M., Blake, D. R., Jonsson, H. H., Lagrosas, N. D., Xian, P., Reid, E. A., Sessions, W. R., and Simpas, J. B.: Size-resolved aerosol and cloud condensation nuclei (CCN) properties in the remote marine South China Sea – Part 1: Observations and source classification, Atmos. Chem. Phys., 17, 1105–1123. https://doi.org/10.5194/acp-17-1105-2017, 2019.

Atwood, S.A., Kreidenweis, S.M., DeMott, P.J., Petters, M.D., Cornwell, G.C., Martin, A.C., and Moore, K.A.: Classification of aerosol population type and cloud condensation nuclei properties in a coastal California littoral environment using an unsupervised cluster model, Atmos. Chem. Phys., 19, 6931–6947, https://doi.org/10.5194/acp-19-6931-2019, 2019.

Bah, M. K., Gunshor, M.M., and Schmit, T.J.: Generation of GOES-16 true color imagery without a green band. *Earth and Space Science*, 5, 549–558. https://doi.org/10.1029/2018EA000379, 2018.

Bryan, G. H., and Fritsch, J.M.: A Benchmark Simulation for Moist Nonhydrostatic Numerical Models. Monthly Weather Review, 130(12), 2917-2928. https://doi.org/10.1175/1520-0493(2002)130<2917:ABSFMN>2.0.CO;2, 2002.

Chandrakar, K. K., Morrison, H., Grabowski, W.W., and Bryan, G.H.: Comparison of Lagrangian Superdroplet and Eulerian Double-Moment Spectral Microphysics Schemes in Large-Eddy Simulations of an Isolated Cumulus Congestus Cloud, J. Atmos. Sci., 79, 1887–1910, https://doi.org/10.1175/JAS-D-21-0138.1, 2022.

Deardorff, J.W.: Stratocumulus-capped mixed layers derived from a three-dimensional model, Boundary-Layer Meteorol. 18, 495–527, https://doi.org/10.1007/BF00119502, 1980.

Dowell, D.C., Alexander, C.R., James, E.P., Weygandt, S.S., Benjamin, S.G., Manikin, G.S., Blake, B.T., Brown, J.M., Olson, J.B., Hu, M., Smirnova, T.G., Ladwig, T., Kenyon, J.S., Ahmadov, R., Turner, D.D., Duda, J.D., and Alcott, T.I.: The High-Resolution Rapid Refresh (HRRR): An Hourly Updating Convection-Allowing Forecast Model. Part I: Motivation and System Description. Weather and Forecasting, 37(8), 1371-1395. https://doi.org/10.1175/WAF-D-21-0151.1, 2022

Fan, J., Wang, Y., Rosenfeld, D., and Liu, X.: Review of Aerosol–Cloud Interactions: Mechanisms, Significance, and Challenges, J. Atmos. Sci., 73, 4221–4252, https://doi.org/10.1175/JAS-D-16-0037.1, 2016.

https://doi.org/10.5194/egusphere-2026-3116
Preprint. Discussion started: 3 July 2026

Fan, J., Rosenfeld, D., Zhang, Y., Giangrande, S.E., Li, Z., Machado, L.A.T., Martin, S.T., Yang, Y., Wang, J., Artaxo, P., Barbosa, H.M.J., Braga, R.C., Comstock, J.M., Feng, Z., Gao, W., Gomes, H.B., Mei, F., Pöhlker, C., Pöhlker, M.L., Pöschl, U., and de Souza, R.A.F.: Substantial convection and precipitation enhancements by ultrafine aerosol particles, Science, 359, 411–418, https://doi.org/10.1126/science.aan8461, 2018.

Fitzgerald, J.W.: Marine aerosols: A review, Atmospheric Environment. Part A. General Topics, 25(3-4), 533-545, https://doi.org/10.1016/0960-1686(91)90050-H, 1991.

Flores, J. M., Bourdin, G., Altaratz, O., Trainic, M., Lang-Yona, N., Dzimban, E., Steinau, S., Tettich, F., Planes, S., Allemand, D., Agostini, S., Banaigs, B., Boissin, E., Boss, E., Douville, E., Forcioli, D., Furla, P., Galand, P. E., Sullivan, M. B., Gilson, É., Lombard, F., Moulin, C., Pesant, S., Poulain, J., Reynaud, S., Romac, S., Sunagawa, S., Thomas, O.P., Troublé, R., de Vargas, C., Vega Thurber, R., Voolstra, C.R., Wincker, P., Zoccola, D., Bowler, C., Gorsky, G., Rudich, Y., Vardi, A., and Koren, I.: Tara Pacific Expedition's Atmospheric Measurements of Marine Aerosols across the Atlantic and Pacific Oceans: Overview and Preliminary Results, Bulletin of the American Meteorological Society, 101, E536-E554, https://doi.org/10.1175/BAMS-D-18-0224.1, 2020.

Forster, P., Storelvmo, T., Armour, K., Collins, W., Dufresne, J.-L., Frame, D., Lunt, D.J., Mauritsen, T., Palmer, M.D., Watanabe, M., Wild, M., and Zhang, H.: The Earth's Energy Budget, Climate Feedbacks, and Climate Sensitivity. In Climate Change 2021: The Physical Science Basis. Contribution of Working Group I to the Sixth Assessment Report of the Intergovernmental Panel on Climate Change [Masson-Delmotte, V., P. Zhai, A. Pirani, S.L. Connors, C. Péan, S. Berger, N. Caud, Y. Chen, L. Goldfarb, M.I. Gomis, M. Huang, K. Leitzell, E. Lonnoy, J.B.R. Matthews, T.K. Maycock, T. Waterfield, O. Yelekçi, R. Yu, and B. Zhou (eds.)]. Cambridge University Press, Cambridge, United Kingdom and New York, NY, USA, pp. 923–1054, https://doi.org/10.1017/9781009157896.009, 2021.

Grabowski, W. W., Morrison, H., Shima, S., Abade, G. C., Dziekan, P., and Pawlowska, H.: Modeling of Cloud Microphysics: Can We Do Better?, Bull. Amer. Meteor. Soc., 100, 655–672, https://doi.org/10.1175/BAMS-D-18-0005.1, 2019.

Hall, W. D.: A Detailed Microphysical Model Within a Two-Dimensional Dynamic Framework: Model Description and Preliminary Results, J. Atmos. Sci., 37, 2486–2507, https://doi.org/10.1175/1520-0469(1980)037<2486:ADMMWA>2.0.CO;2, 1980.

Huang, Y., McFarquhar, G. M., Patil, S. U., Gao, L., Taszarek, M., Xue, M., Dzambo, A., Wolde, M., Nichman, L., Nguyen, C., Ranjbar, K., Bliankinshtein, N., Bala, K., Kollias, P., Jensen, M. P., Mo, Q., Bruintjes, R., Kuang, C., and Subba, T.: Dependence of Convective Cloud Microphysical Properties on Environmental Conditions during the TRACER and ESCAPE Field Campaigns: A Synergistic Approach of Observations, Machine Learning, and Parcel Models, J. Atmos. Sci., 82, 2291–2312, https://doi.org/10.1175/JAS-D-24-0269.1, 2025.

Iacono, M. J., Delamere, J. S., Mlawer, E. J., Shephard, M. W., Clough, S. A., and Collins, W. D.: Radiative forcing by long-lived greenhouse gases: Calculations with the AER radiative transfer models, J. Geophys. Res., 113, D13103, https://doi.org/10.1029/2008JD009944, 2008.

https://doi.org/10.5194/egusphere-2026-3116
Preprint. Discussion started: 3 July 2026

Igel, A. L., and van den Heever, S. C.: Invigoration or enervation of convective clouds by aerosols? Geophysical Research Letters, 48, e2021GL093804. https://doi.org/10.1029/2021GL093804, 2021.

Im, U., Samset, B. H., Nenes, A., Thomas, J. L., Kokkola, H., Dubovik, O., Amiridis, V., Arola, A., Bellouin, N., Benedetti, A., Bilde, M., Blichner, S., Decesari, S., Ekman, A.M.L., García-Pando, C.P., Gross, S., Gryspeerdt, E., Hasekamp, O., Kahn, R.A., Laakso, A., Lohmann, U., Marelle, L., Massling, A.H., Myhre, C.L., Pöhlker, M., Quaas, J., Raatikainen, T., Riipinen, I., Schmale, J., Seifert, P., Skov, H., Smith, C., Sporre, M.K., Stier, P., Storelvmo, T., Tsigaridis, K., van Diedenhoven, B., Virtanen, A., Wandinger, U., Wilcox, L.J., and Zieger, P.: Aerosol-cloud interactions: Overcoming a barrier to projecting near-term climate evolution and risk, AGU Advances, 7, e2025AV001872. https://doi.org/10.1029/2025AV001872, 2026.

Jensen, M.P., Collins, D., Kollias, P., Rosenfeld, D., Varble, A., Collis, S.M., Fan, J., Griffin, R., Jackson, R.C., Logan, T., McFarquhar, G., Quaas, J., Sheesley, R., Stier, P., van den Heever, S., Wang, Y., Zhang, G., Bruning, E., Fridlind, A., Kuang, C., Ryzhkov, A., Brooks, S., Defer, E., Giangrande, S.E., Hu, J., Kumjian, M., Matsui, T., Nowotarski, C., Oue, M., Snyder, J., Usenko, S., van Lier-Walqui, M., and Xu, Y.: Tracking Aerosol Convection Interactions Experiment (TRACER) Science Plan. Brookhaven National Laboratory Tech. Rep. BNL-212068-2019-INRE, 41 pp., https://doi.org/10.2172/1561242, 2019.

Jensen, M.P., Flynn, J.H., Kollias, P., Kuang, C., McFarquhar, G., Powers, H., Brooks, S., Bruning, E., Collins, D., Collis, S.M., Fan, J., Fridlind, A., Giangrande, S.E., Griffin, R., Hu, J., Jackson, R.C., Kumjian, M., Logan, T., Matsui, T., Nowotarski, M. Oue, A. Rapp, D. Rosenfeld, A. Ryzhkov, R. Sheesley, J. Snyder, P. Stier, S. Usenko, S. van den Heever, M. van Lier-Walqui, C., Varble, A., Wang, Y., Aiken, A., Deng, M., Dexheimer, D., Dubey, M., Feng, Y., Ghate, V., Johnson, K., Lamer, K., Saleeby, S., Wang, D., Zawadowicz, M., and Zhou, A.: Tracking Aerosol Convection Interactions Experiment (TRACER) Field Campaign Report. U.S. Department of Energy, Atmospheric Radiation Measurement user facility, Richland, Washington. DOE/SC-ARM-23-038, https://doi.org/10.2172/2202672, 2023.

Jensen, M. P., Flynn, J. H., Gonzalez-Cruz, J. E., Judd, L. M., Kollias, P., Kuang, C., McFarquhar, G. M., Powers, H., Ramamurthy, P., Sullivan, J., Aiken, A. C., Alvarez, S. L., Argay, P., Argrow, B., Bell, T. M., Boyer, D., Brooks, S. D., Bruning, E. C., Brunner, K., Butterworth, B., Calmer, R., Cappa, C. D., Chakrabarty, R. K., Chandrasekar, V., Chao, C., Chen, B., China, S., Collins, D. R., Collis, S. M., Crowell, S., Porto, R. D., Boer, G. d., Deng, M., Dexheimer, D., Drager, A. J., Du, X., Dubey, M. K., Dzambo, A. M., Etten-Bohm, M., Fan, J., Farley, R., Feng, Y., Feng, Y., Fenn, M., Ferrare, R. E., Flusche, S., Fridlind, A. M., Galewsky, J., Gamarro, H., Gardner, S., Ghate, V. P., Giangrande, S. E., Griffin, R. J., Griggs, T., Gronoff, G. P., Grover, M., Gaugenti, M., Guo, F., Gupta, S., Hu, J., Huang, Y., Jackson, R. C., Hair, J. W., Johnson, K. L., Kasparoglu, S., Klein, P., Kotsakis, A. E., Kumar, J., Kumjian, M. R., Lamer, K., Lappin, F. M., Lei, Z., Li, J., Li, R., Li, Y., Logan, T., Lombardo, K., Luke, E. P., Mages, Z., Matthews, A. A., Matthews, B. H., Mayol-Bracero, O., Matsui, T., McKeown, K. E., Mehra, M., Mei, F., Meskidzhe, N., Nguyen, C., Nielsen, E. R., Nowotarski, C. J., Oaks, D., Oktem, R., Oue, M., Park, J. M., Partida, N., Patil, S., Pena, J. C., Petters, M. D., Phoenix, D. B., Puthserry, J. V., Rapp, A. D., Romps, D. M., Roots, M., Rosenfeld, D., Saleeby, S. M., Savala, P., Sedlacek, A. J., Sharma, M., Sheesley, R., Shingler, T. J., Shrestha, S., Singh, A., Smith, E. N., Smith, J. N., Smith, S., Snyder, J., Spicer, E., Spinei, E., Spychala, M., Steir, P., Storm, M. R., Subba, T., Treserras, B. P., Trojanowski, R., Theisen, A., Thompson, S. A., Twigg, L., Uin, J., Ulinski, A. R., van den Heever, S., van

https://doi.org/10.5194/egusphere-2026-3116
Preprint. Discussion started: 3 July 2026

Lier-Walqui, M., Varble, A. C., Wagner, T. J., Wakeen, J., Wales, N. A., Walter, P. J., Wang, D., Wang, J., Wood, L., Wang, Y., Wolde, M., Yoon, S., Young, M. H., Zawadowicz, M. A., Zhang, Q., Zhou, A., Zhu, Z., and Zhu, Z.: Studying Aerosol, Clouds, and Air Quality in the Coastal Urban Environment of Southeastern Texas, Bull. Amer. Meteor. Soc., BAMS-D-23-0331.1, https://doi.org/10.1175/BAMS-D-23-0331.1, 2025.

Khain, A. P., Beheng, K. D., Heymsfield, A., Korolev, A., Krichak, S.O., Levin, Z., Pinsky, M., Phillips, V., Prabhakaran, T., Teller, A., van den Heever, S. C., Yano, J.-I.: Representation of microphysical processes in cloud-resolving models: Spectral (bin) microphysics versus bulk parameterization, Rev. Geophys., 53, 247–322, https://doi.org/10.1002/2014RG000468, 2015.

Khairoutdinov, M., and Kogan, Y.: A New Cloud Physics Parameterization in a Large-Eddy Simulation Model of Marine Stratocumulus, Mon. Wea. Rev., 128, 229–243, https://doi.org 10.1175/1520-0493(2000)128<0229:ANCPPI>2.0.CO;2, 2000.

Koponen, I. K., Virkkula, A., Hillamo, R., Kerminen, V.-M., and Kulmala, M.: Number size distributions and concentrations of marine aerosols: Observations during a cruise between the English Channel and the coast of Antarctica, J. Geophys. Res., 107(D24), 4753. https://doi.org/10.1029/2002JD002533, 2002.

Lebo, Z. J. and Seinfeld, J. H.: Theoretical basis for convective invigoration due to increased aerosol concentration, Atmos. Chem. Phys., 11, 5407–5429, https://doi.org/10.5194/acp-11-5407-2011, 2011.

Li, T., Yu, Y., Wang, X., Liu, X., Mao, Q., and Yuan, Y.: A review of aerosol-cloud interactions: Mechanisms, climate effects, and observation methods, Atmospheric Research, 325, 108267, https://doi.org/10.1016/j.atmosres.2025.108267, 2025.

Mages, Z., Kollias, P., Treserras, B. P., Borque, P., and Oue, M.: Shallow cloud variability in Houston, Texas, during the ESCAPE and TRACER field experiments, Atmos. Chem. Phys., 25, 6025–6045, https://doi.org/10.5194/acp-25-6025-2025, 2025.

Marinescu, P. J., van den Heever, S. C., Heikenfeld, M., Barrett, A. I., Barthlott, C., Hoose, C., Fan, J., Fridlind, A. M., Matsui, T., Miltenberger, A. K., Stier, P., Vie, B., White, B. A., and Zhang, Y.: Impacts of Varying Concentrations of Cloud Condensation Nuclei on Deep Convective Cloud Updrafts—A Multimodel Assessment, J. Atmos. Sci., 78, 1147–1172, https://doi.org/10.1175/JAS-D-20-0200.1, 2021.

Morrison, H., Curry, J.A., and Khvorostyanov, V.I.: A New Double-Moment Microphysics Parameterization for Application in Cloud and Climate Models. Part I: Description, Journal of the Atmospheric Sciences, 62(6), 1665-1677. https://doi.org/10.1175/JAS3446.1, 2005.

Morrison, H., Thompson, G., and Tatarskii, V.: Impact of Cloud Microphysics on the Development of Trailing Stratiform Precipitation in a Simulated Squall Line: Comparison of One- and Two-Moment Schemes, Monthly Weather Review, 137(3), 991-1007. https://doi.org/10.1175/2008MWR2556.1, 2009.

Morrison, H., Witte, M., Bryan, G. H., Harrington, J. Y., and Lebo, Z. J.: Broadening of Modeled Cloud Droplet Spectra Using Bin Microphysics in an Eulerian Spatial Domain, J. Atmos. Sci., 75, 4005–4030, https://doi.org/10.1175/JAS-D-18-0055.1, 2018.

Morrison, H., van Lier-Walqui, M., Fridlind, A. M., Grabowski, W. W., Harrington, J. Y., Hoose, C., Korolev, A., Kumjian, M.R., Milbrandt, J.A., Pawlowska, H., Posselt, D.J., Prat, O.P., Reimel, K.J., Shima, S.-I., van Diedenhoven, B., and Xue, L.:

https://doi.org/10.5194/egusphere-2026-3116
Preprint. Discussion started: 3 July 2026

Confronting the challenge of modeling cloud and precipitation microphysics, Journal of Advances in Modeling Earth Systems, 12, e2019MS001689, https://doi.org/10.1029/2019MS001689, 2020.

Mülmenstädt, J., Salzmann, M., Kay, J.E., Zelinka, M.D., Ma, P.-L., Nam, C., Kretzschmar, J., Hörnig, S., and Quaas, J.: An underestimated negative cloud feedback from cloud lifetime changes, Nat. Clim. Chang., 11, 508–513, https://doi.org/10.1038/s41558-021-01038-1, 2021.

Naumann, A. K., and Seifert, A.: A Lagrangian drop model to study warm rain microphysical processes in shallow cumulus, J. Adv. Model. Earth Syst., 7, 1136–1154, https://doi.org/10.1002/2015MS000456, 2015.

NOAA Geostationary Operational Environmental Satellites (GOES) 16, 17, 18, and 19 was accessed on December 23, 2025, from https://registry.opendata.aws/noaa-goes.

Öktem, R., Romps, D. M., and Varble, A. C.: No Warm-Phase Invigoration of Convection Detected during GoAmazon, J. Atmos. Sci., 80, 2345–2364, https://doi.org/10.1175/JAS-D-22-0241.1, 2023.

Park, J. M., van den Heever, S. C., Igel, A. L., Grant, L. D., Johnson, J. S., Saleeby, S. M., Miller, S.D., Reid, J.S.: Environmental controls on tropical sea breeze convection and resulting aerosol redistribution, Journal of Geophysical Research: Atmospheres, 125, e2019JD031699. https://doi.org/10.1029/2019JD031699, 2020.

Patil, S., McFarquhar, G., Huang, Y., Roberts, G., Wolde, M., Nichman, L., Nguyen, C.M., Ranjbar, K., Bliankinshtein, N., Richter, A., Kollias, P., and Rosenfeld, D.: Quasi-Steady State Supersaturation: Do High Values Derived from ESCAPE Represent Real High Supersaturations and the Potential for Condensational Invigoration?, ESS Open Archive, https://doi.org/10.22541/essoar.176031289.91390863/v1, 2025.

Pöhlker, M.L., Pöhlker, C., Quaas, J., Mülmenstädt, J., Pozzer, A., Andreae, M.O., Artaxo, P., Block, K., Coe, H., Ervens, B., Gallimore, P., Gaston, C.J., Gunthe, S.S., Henning, S., Herrmann, H., Krüger, O.O., McFiggans, G., Poulain, L., Raj, S.S., Reyes-Villegas, E., Royer, H.M., Walter, D., Wang , Y., and Pöschl, U.: Global organic and inorganic aerosol hygroscopicity and its effect on radiative forcing, Nature Communications, 14, 6139, https://doi.org/10.1038/s41467-023-41695-8, 2023.

Petters, M.D., and Kreidenweis, S.M.: A single parameter representation of hygroscopic growth and cloud condensation nucleus activity, Atmos. Chem. Phys., 7, 1961–1971, https://doi.org/10.5194/acp-7-1961-2007, 2007.

Ralph, F. M., Prather, K.A., Cayan, D., Spackman, J.R., DeMott, P., Dettinger, M., Fairall, C., Leung, R., Rosenfeld, D., Rutledge, S., Waliser, D., White, A.B., Cordeira, J., Martin, A., Helly, J., and Intrieri, J.: CalWater Field Studies Designed to Quantify the Roles of Atmospheric Rivers and Aerosols in Modulating U.S. West Coast Precipitation in a Changing Climate, Bulletin of the American Meteorological Society, 97(7), 1209-1228. https://doi.org/10.1175/BAMS-D-14-00043.1, 2016.

Roberts, G.C., Ranjbar, K., Nichman, L., Wolde, M., McCluskey, C.S., Takeishi, A., Patnaude, R., Allwayin, N., Shaw, R., Patil, S., McFarquhar, G., and Kollias, P.: Marine aerosol to refinery emissions: Transport and evolution of CCN in the Houston Metropolitan area and their impact on cloud formation, Journal of Geophysical Research: Atmospheres, https://doi.org/10.1029/2025JD044628, 2026.

Rolph, G., Stein, A., and Stunder, B.: Real-time Environmental Applications and Display sYstem: READY, Environmental Modelling & Software, 95, 210-228. https://doi.org/10.1016/j.envsoft.2017.06.025, 2017.

https://doi.org/10.5194/egusphere-2026-3116
Preprint. Discussion started: 3 July 2026

Rosenfeld, D., Lohmann, U., Raga, G.B., O'Dowd, C.D., Kulmala, M., Fuzzi, S., Reissell, A., and Andreae, M.O.: Flood or Drought: How Do Aerosols Affect Precipitation?, Science, 321, 1309-1313. https://doi.org/10.1126/science.1160606, 2008.

Rousseeuw, P.J.: Silhouettes: A graphical aid to the interpretation and validation of cluster analysis, Journal of Computational and Applied Mathematics, 20, 53-65, https://doi.org/10.1016/0377-0427(87)90125-7, 1987.

Saleeby, S. M., van den Heever, S.C., Marinescu, P.J., Oue, M., Barrett, A.I., Barthlott, C., Cherian, R., Fan, J., Fridlind, A.M., Heikenfeld, M., Hoose, C., Matsui, T., Miltenberger, A.K., Quaas, J., Shpund, J., Stier, P., Vie, B., White, B.A., and Zhang, Y.: Model Intercomparison of the Impacts of Varying Cloud Droplet–Nucleating Aerosols on the Life Cycle and Microphysics of Isolated Deep Convection, Journal of the Atmospheric Sciences, 82(10), 2197-2217, https://doi.org/10.1175/JAS-D-24-0181.1, 2025.

Sato, Y., Nishizawa, S., Yashiro, H., Miyamoto, Y., Kajikawa, Y., and Tomita, H.: Impacts of cloud microphysics on trade wind cumulus: which cloud microphysics processes contribute to the diversity in a large eddy simulation?, Prog. in Earth and Planet. Sci., 2, 23, https://doi.org/10.1186/s40645-015-0053-6, 2015.

Sato, Y., Shima, S., and Tomita, H.: Numerical convergence of shallow convection cloud field simulations: Comparison between double-moment Eulerian and particle-based Lagrangian microphysics coupled to the same dynamical core, Journal of Advances in Modeling Earth Systems, 10, 1495–1512. https://doi.org/10.1029/2018MS001285, 2018.

Schmit, T. J., Griffith, P., Gunshor, M.M., Daniels, J.M., Goodman, S.J., and Lebair, W.J.: A Closer Look at the ABI on the GOES-R Series, Bulletin of the American Meteorological Society, 98(4), 681-698, https://doi.org/10.1175/BAMS-D-15-00230.1, 2017.

Shima, S., Kusano, K., Kawano, A., Sugiyama, T., and Kawahara, S.: The super-droplet method for the numerical simulation of clouds and precipitation: a particle-based and probabilistic microphysics model coupled with a non-hydrostatic model, Q.J.R. Meteorol. Soc., 135: 1307-1320. https://doi.org/10.1002/qj.441, 2009.

Stanford, M. W., Fridlind, A. M., Ackerman, A. S., van Diedenhoven, B., Xiao, Q., Wang, J., Matsui, T., Hernandez-Deckers, D., and Lawson, P.: Warm-phase microphysical evolution in large-eddy simulations of tropical cumulus congestus: evaluating drop size distribution evolution using polarimetry retrievals, in situ measurements, and a thermal-based framework, Atmos. Chem. Phys., 25, 11199–11231, https://doi.org/10.5194/acp-25-11199-2025, 2025.

Stein, A.F., Draxler, R.R., Rolph, G.D., Stunder, B.J.B., Cohen, M.D., and Ngan, F.: NOAA's HYSPLIT atmospheric transport and dispersion modeling system, Bull. Amer. Meteor. Soc., 96, 2059-2077, http://dx.doi.org/10.1175/BAMS-D-14-00110.1, 2015.

Subba, T., Jensen, M. P., Deng, M., Giangrande, S. E., Harvey, M. C., Singh, A., Wang, D., Zawadowicz, M., and Kuang, C.: Implications of Sea Breeze Circulations on Boundary Layer Aerosols in the Southern Coastal Texas Region, Atmos. Chem. Phys., 26, 2853–2879, https://doi.org/10.5194/acp-26-2853-2026, 2026.

Thompson, S. A., Chen, B., Matthews, B. H., Li, R., Nowotarski, C. J., Rapp, A. D., and Brooks, S. D: Characterizing Greater Houston's aerosol by air mass during TRACER, Journal of Geophysical Research: Atmospheres, 130, e2025JD043353. https://doi.org/10.1029/2025JD043353, 2025a.

https://doi.org/10.5194/egusphere-2026-3116
Preprint. Discussion started: 3 July 2026

Thompson, S. A., Peña, T. A., Chen, B., Sharma, M., Matthews, B. H., Li, R., Nowotarski, C.J., Rapp, A.D., and Brooks, S.D.: Variability in ice nucleating particles across Greater Houston Texas, Journal of Geophysical Research: Atmospheres, 130, e2025JD044164. https://doi.org/10.1029/2025JD044164, 2025b.

Thorndike, R.L.: Who belongs in the family?. Psychometrika, 18, 267–276. https://doi.org/10.1007/BF02289263, 1953.

Tuftedal, K. S., Treserras, B. P., Oue, M., and Kollias, P.: Shallow- and deep-convection characteristics in the greater Houston, Texas, area using cell tracking methodology, Atmos. Chem. Phys., 24, 5637–5657, https://doi.org/10.5194/acp-24-5637-2024, 2024.

Varble, A. C., Igel, A. L., Morrison, H., Grabowski, W. W., and Lebo, Z. J.: Opinion: A critical evaluation of the evidence for aerosol invigoration of deep convection, Atmos. Chem. Phys., 23, 13791–13808, https://doi.org/10.5194/acp-23-13791-2023, 2023.

Wang, D., Melvin, E. C., Smith, N., Jensen, M. P., Gupta, S., Abdullah-Smoot, A., Pszeniczny, N., and Hahn, T.: TRACER Perspectives on Gulf-Breeze and Bay-Breeze Circulations and Coastal Convection, Mon. Wea. Rev., 152, 2207–2228, https://doi.org/10.1175/MWR-D-23-0292.1, 2024.

Wang, D., Kobrosly, R., Zhang, T., Subba, T., van den Heever, S., Gupta, S., and Jensen, M.: Aerosol impacts on isolated deep convection: findings from TRACER, Atmos. Chem. Phys., 25, 9295–9314, https://doi.org/10.5194/acp-25-9295-2025, 2025.

Witte, M. K., Morrison, H., Davis, A. B., and Teixeira, J.: Limitations of Bin and Bulk Microphysics in Reproducing the Observed Spatial Structure of Light Precipitation, J. Atmos. Sci., 79, 161–178, https://doi.org/10.1175/JAS-D-21-0134.1, 2022.

Yin, C., Shima, S., Xue, L., and Lu, C.: Simulation of marine stratocumulus using the super-droplet method: numerical convergence and comparison to a double-moment bulk scheme using SCALE-SDM 5.2.6-2.3.1, Geosci. Model Dev., 17, 5167–5189, https://doi.org/10.5194/gmd-17-5167-2024, 2024.

Zhang, Y., Fan, J., Li, Z., and Rosenfeld, D.: Impacts of cloud microphysics parameterizations on simulated aerosol–cloud interactions for deep convective clouds over Houston, Atmos. Chem. Phys., 21, 2363–2381, https://doi.org/10.5194/acp-21-2363-2021, 2021.